1. Helioseismology

1.1. Introduction

Small amplitude oscillations of the Sun with a period of about 5 minutes were discovered by Bob Leighton (prof. physics, Caltech) and collaborators in 1962. The first really good and extensive list of Solar mode frequencies was generated by Ken Libbrecht and Bob Woodward from observations made at Big Bear Solar Observatory, started by astronomy prof. emeritus Hal Zirin.

Following on these pioneering efforts, an international network of telescopes arranged around the earth in latitude so that the Sun never sets was started in about 1996 by the National Solar Observatory (a NSF funded US institution) to observe solar oscillations. The GONG project (Global Oscillation Network Project) is still running today; see their website at gong.nso.edu. In addition there are a number of satellites that have been launched to study these phenomena, including an instrument called GOLF on SOHO (Solar and Heliospheric Observatory) (sohowww.nascom.nasa.gov), a collaboration between NASA and ESA launched in 1995.

These small amplitude waves are very difficult to detect. In the Sun periods range from 3 to 12 min, but the vertical velocity amplitude of a single mode is only $\sim$3 cm/sec. Many modes are present at a given time, and the maximum surface motions have an amplitude of 1 km/sec.

Such periodic oscillations are observed in the Sun taking advantage of our ability to observe the entire surface (or more correctly half of the surface at a given time) of the Sun. Radial velocities measured from studying absorption lines, the equivalent widths of temperature sensitive lines, or high precision photometry over the surface, are measured on timescales short compared to 3 min, with continuous monitoring over many months or

years. The resulting data sets are Fourier transformed to study the modes of oscillation.

A number of satellites with small telescopes have been launched to detect such oscillations in nearby stars; this field is called asteroseismology in analogy to helioseismology. These include MOST (Microvariability and Oscillation of Stars), built by Canada and launched in 2003. It has a telescope with diameter 15 cm and observes through a single broad-band filter which covers from 350 to 700 nm. COROT was built by France with several international collaborators. COROT was launched in Dec. 2006, and contains a 23 cm diameter telescope. It can detect a periodic change in brightness at 500 nm (5000 Å) of 1 part in 10^6 for a 6th mag star with a period of a few days. Such sensitivity cannot be achieved from the ground, except for the Sun.

1.2. The Speed of Sound in a Uniform Gas

We begin by deriving the speed of pressure waves in a gas whose equilibrium temperature, density and pressure are independent of position. Pressure waves with a frequency within the range that can be detected by human ears are called acoustic or sound waves. Pressure waves represent oscillations in pressure where the oscillation is in the direction of travel of the wave. Waves where the oscillation is perpendicular to the direction of travel of the wave, such as ocean waves, are called gravity waves. These are abbreviated as p and g waves.

Initially the gas has pressure P_0, density ρ_0 at all points, and is assumed to be at rest. To calculate the oscillation, we need three equations. They are:

(I) the gas moves, this changes ρ

(II) the change in density produces a change in pressure

(III) pressure inequalities produce a force which leads to motion of the gas

The equilibrium values are denoted with subscript 0, the perturbed values are denoted with superscripts 1. The equilibrium velocity is 0, so v denotes the motion of the gas due to the perturbation. In this derivation we retain terms which are first order in the perturbation, but ignore second order perturbation terms as they will be much smaller.

We assume that the period of oscillation is short compared with the time required for heat to be exchanged with the surrounding material, and hence the oscillations are adiabatic. Thus we already know the form of the second equation.

Since we assume an adiabatic process, the second equation is derived from $P \propto \rho^{\gamma}$. This implies:

$$\frac{dP}{P} = \frac{\gamma d\rho}{\rho}. \quad (eq.\ II)$$

The form of this equation for the perturbed gas is:

$$\frac{P^1}{P_0} = \frac{\gamma \rho^1}{\rho_0} \quad (eq.\ IIp).$$

The first equation is the mass continuity equation (ρv = constant). Since the laws of physics apply to the individual fluid particles, we must follow them within the fluid, and use the Lagrangian form for the derivitives, so that

$$\frac{d}{dt} = \frac{\partial}{\partial t} + v\frac{\partial}{\partial x},$$

where the partial derivatives refer to changes at a fixed point.

Equation 1 is thus

$$\frac{\partial \rho}{\partial t} + \frac{\partial(\rho v)}{\partial x} = 0 \quad (eq.\ I)$$

Equation 1, for the perturbed gas, becomes:

$$\frac{\partial \rho^1}{\partial t} + \frac{\partial[(\rho_0 + \rho^1)v]}{\partial x} = 0$$

Eliminating the second order term, equation Ip is:

$$\frac{\partial \rho^1}{\partial t} = -\rho_0 \frac{\partial v}{\partial x} \quad (eq.\ Ip).$$

Now we need the force equation (equation III). The pressure force per unit volume is $-\partial P/\partial x$. If we denote the external force per unit volume (if present) as $f(ext)$, then Newton's Law states:

$$\rho \frac{dv}{dt} + \frac{\partial P}{\partial x} = f(ext)$$

This becomes:

$$\frac{\partial v}{\partial t} + \frac{v \partial v}{\partial x} + \frac{1}{\rho}\frac{\partial P}{\partial x} = \frac{f}{\rho} \quad (eq.\ III)$$

.

We set the external force to 0 and perturb the gas, to get

$$\rho_0 \frac{\partial v}{\partial t} + \rho^1 \frac{\partial v}{\partial t} + \frac{\partial P^1}{\partial x} = 0.$$

We ignore the second term, which is second order, to get:

$$\frac{\partial v}{\partial t} \;=\; -\frac{1}{\rho_0}\frac{\partial P^1}{\partial x} \qquad (eq.\ IIIp).$$

We now have the three required equations set up for the perturbed gas. We need to combine them to eliminate variables to end up with an equation for either P^1 or ρ^1. We combine eq. Ip and IIp to get

$$\frac{\partial \rho^1}{\partial t} \;=\; -\;\rho_0\,\frac{\partial v}{\partial x} \;\text{ becomes }\; \frac{1}{\gamma P_0}\frac{\partial P^1}{\partial t} \;=\; -\;\frac{\partial v}{\partial x} \quad (eq.\ Ip + IIp)$$

We now use eq. IIIp and differentiate, to get:

$$\frac{\partial}{\partial x}[\frac{\partial P^1}{\partial x} \;+\; \rho_0\frac{\partial v}{\partial t}] \;=\; 0.$$

Substituting in from eq. Ip+IIp, we end up with the wave equation:

$$\frac{\partial^2 P^1}{\partial x^2} \;+\; \frac{\rho_0}{\gamma P_0}\frac{\partial^2 P^1}{\partial t^2} \;=\; 0.$$

The solution to this equation is a wave, $Ae^{i(kx-\omega t)}$ whose velocity is the speed of sound, c_s, where

$$c_s^2 \;=\; \frac{\gamma P_0}{\rho_0} \;=\; \frac{\gamma k T_0}{\mu m_H}.$$

Note that c_s is approximately $\gamma/3 \times$ the mean speed of a particle in the gas.

1.3. Acoustic Waves in Stars

The above derivation is too simple to use for a star. We first relax the assumption of constant density, and consider an isothermal atmosphere with a constant gravity. This is

assumed to be in hydrostatic equilibrium, and hence has

$$\rho(z) \;=\; \rho_0 e^{-z/H},$$

where H is the pressure scale height, $H = kT/(\mu m_H g)$. This introduces one additional term into the wave equation, which becomes

$$\frac{\partial^2 z'}{\partial t^2} \;=\; c_s^2 \frac{\partial^2 z'}{\partial z^2} \;-\; \frac{c_s^2}{H}\frac{\partial z'}{\partial z}.$$

The last term is the new one, and its presence complicates the solution.

We seek a sinusoidal solution to this equation. We expect the energy of the wave to remain constant as the wave propagates upward in the star at constant velocity while the density decreases. So we try

$$z^1(z,t) \;=\; \frac{Z(z)e^{i\omega t}}{\sqrt{\rho(z)}}$$

We get a differential equation for $Z(z)$,

$$\frac{d^2 Z}{dz^2} \;+\; Z\,\frac{(\omega^2 - \omega_c^2)}{c_s^2} \;=\; 0,$$

where the critical frequency, $\omega_c = c_s/(2H)$. Then $Z(z) = Aexp(-ikz)$ is a solution to the above differential equation provided that

$$k \;=\; +\sqrt{\frac{(\omega^2 - \omega_c^2)}{c_s^2}} \;\text{ or }\quad -\sqrt{\frac{(\omega^2 - \omega_c^2)}{c_s^2}}.$$

Positive k corresponds to a wave attempting to propagate vertically upward, while negative k corresonds to a wave attempting to travel deeper into the atmosphere. We

consider the former (positive k) case.

For $\omega > \omega_c$, a sinusoidal wave propagating upward is obtained. Its amplitude as the wave propagates upward is $A/\sqrt{\rho(z)}$. This increases with time as the density decreases upward. However, for $\omega < \omega_c$ there is an evanescent sinusoidal solution in which the displacement amplitude damps out exponentially as the wave propagates upwards.

Thus $\omega_c = c_s/(2H)$ is a critical frequency below which pressure waves cannot propagate in an isothermal atmosphere with scale height H.

For stars, we also have to relax the assumption of constant temperature, equivalent to constant scale height H. The resulting equations are even more difficult to solve; one ends up with the same general form of solution, but the cutoff frequency is modified to become:

$$\omega_c^2 \;=\; \frac{c_s^2}{4H^2}(1 - 2\frac{dH}{dz}).$$

One more complication needs to be taken into account to treat real stars accurately. We need to relax the assumption that c_s is constant. Since the temperature is not constant, the sound speed becomes a function of position in the atmosphere. We do not attempt that exact case here.

1.4. Gravity Waves in Stars

Gravity waves occur when the displacement of a parcel of gas is perpendicular to the direction of travel of the wave. We already discussed oscillations in a gas displaced vertically. The upward bouyancy force per unit mass (recall the discussion of convection) is

$$F = \frac{g}{\rho}[\Delta\rho - \delta\rho],$$

where $\Delta\rho$ is the difference in bulk atmospheric density while $\delta\rho$ is the same inside the rising gas parcel. If we rewrite F as $F = -N^2\Delta x$, where

$$N^2 = -\frac{g}{\rho}[\frac{\Delta\rho}{\Delta x} - \frac{\delta\rho}{\Delta x}]$$

then when N^2 is positive, we have a wave equation with a sinusoidal solution with frequency N. N is called the Brunt–Vaisala frequency.

We can also write N^2 as

$$N^2 = -g[\frac{\gamma - 1}{\gamma}\frac{1}{P}\frac{dP}{dz} - \frac{1}{T}\frac{dT}{dz}].$$

The propagation of a gravity wave requires that buoyancy oscillations in adjacent elements of the stellar atmosphere be appropriate coordinated. From the above equation, one can show that gravity waves cannot propagate in convection zones.

Thus gravity waves can propagate with frequencies up to N but not in (through) convection zones. Horizontal gravity waves will have angular frequency N. Gravity waves travelling in other directions will be subject to a reduced bouyant force, and hence will have smaller angular frequencies.

1.5. Wave Propagation

Within the Sun the temperature increases rapidly inwards, and thus so does the sound speed, c_s. An average value of c_s for the Sun, adopting $T \sim 6 \times 10^6$ K, is about

4×10^5 m/sec. A pressure wave propagating inwards at an angle with velocity $c_s(z)$ will thus be refracted. (Try drawing wave fronts and you will convince yourself of this.) Such a wave, propagating towards higher T will gradually turn around and head back towards the surface of the star where c_s is lower. The shallower the angle with respect to the surface, the smaller the depth the p-wave reaches.

Recall that pressure waves must have angular frequencies $> \omega_c$, where a typical value of $\omega_c \sim c_s/(2H)$ is $\sim 4 \times 10^{-3}$ radians/sec, corresponding to a maximum period of about 25 minutes.

Pressure waves are reflected at the outer surface of the Sun, once the local value of ω_c, which is decreasing toward the surface, reaches ω. A wave with a period of about 3 minutes ($\omega \sim 3.5 \times 10^{-2}$ radians/sec) cannot propagate at heights more than 500 km above the visual solar surface.

Gravity waves can propagate in the interior of the Sun with $N \sim 3 \times 10^{-3}$ sec^{-1} corresponding to a period of ~ 35 minutes. But N goes to 0 when the lower boundary of the convection zone is reached, and the interior gravity waves cannot propagate higher than that level.

1.6. Waves Inside the Sun

We now consider the normal modes of non-radial oscillation of the Sun. While in principle a pressure or gravity wave can have any ω within the ranges discussed above, in practice only those modes which are resonant will have finite lifetimes.

The center of the Sun must be a node of any wave which reaches that point as by symmetry the point $r = 0$ cannot be displaced.

The resonant modes are a radial function times the spherical harmonics $Y(l,m)$. At first sight the system is spherically symmetic, so that the mode frequency should be a function of n and l only. However, the Solar rotation defines an axis which removes this degeneracy and splits the modes such that the p-mode frequency is slightly different for modes of different m. Each mode is split into $2l+1$ components whose frequencies are separated by the rotational frequency of the Sun, which on average is $\Omega/2\pi \approx 440$ nHz. A star-wide organized magnetic field can also split the modes in this way.

The radial function for the amplitude of a p-mode satisfies the equation:

$$[\frac{1}{r^2}\frac{d}{dr}(r^2\frac{d}{dr}) \; - \; \frac{l(l+1)}{r^2} \; + \; \frac{\omega^2}{c_s^2}]R \; = \; 0.$$

This leads to the identification of the p-modes by their frequency ($\sec^{-1}$) and the horizontal wave number k_h, which indicates the size of 1 wavelength on the solar surface, $k_h = 2\pi/\Delta x$. We set

$$k_h \; = \; \frac{\sqrt{l(l+1)}}{R_\odot},$$

and use l as the degree of oscillation.

The exact solutions of this equation which satisfy the relevant boundary conditions are the eigenvalues of the oscillation problem. For each value of l there are a sequence of modes with radial degree n that have $n-1$ nodes between $r=0$ and $r=R_\odot$. Eigenfunctions with low values of l penetrate deep into the Sun, while those with high values of l have very small amplitudes near the center of the Sun.

The turning radius of the mode r_t of a a wave originating at the surface and propagating downwards, i.e. the radius at which turns to propagate upwards instead, is given in HKT

(equation 8.114) as

$$\frac{c_s(r_t)}{r_t} = \frac{2\pi f_{nl}}{\sqrt{l(l+1)}},$$

where f_{nl} is the frequency of the mode. This is due to refraction as indicated earlier.

Movies of solar oscillation modes can be found at several web sites, for example at the website of the BISON project (Birmingham Solar Oscillations Network, a six telescope/six observatory remotely operated solar monitoring array), bison.ph.bham.ac.uk/about/modes.html.

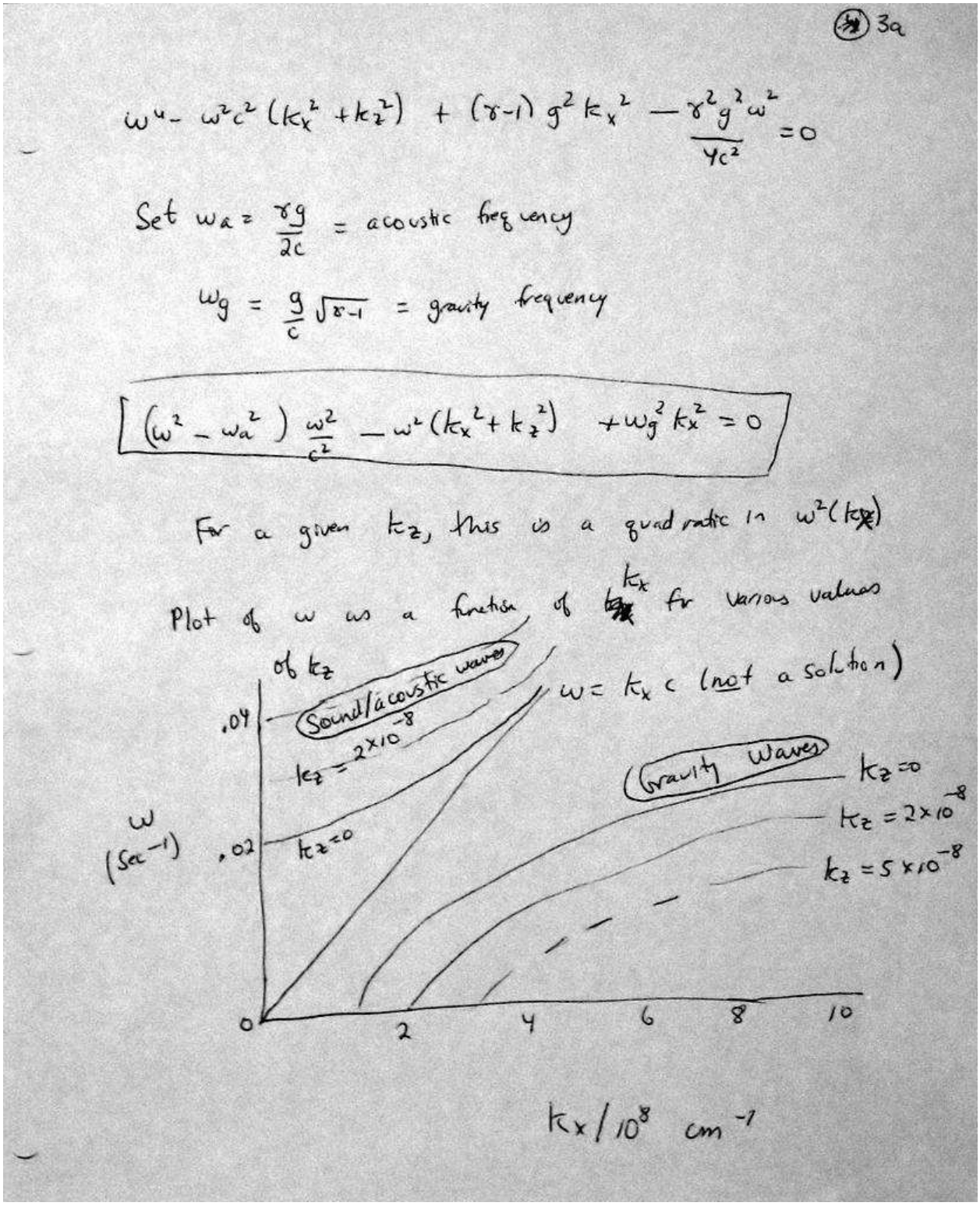

Fig. 1.— Wavenumber versus angular frequency for pressure and gravity waves in the Sun.

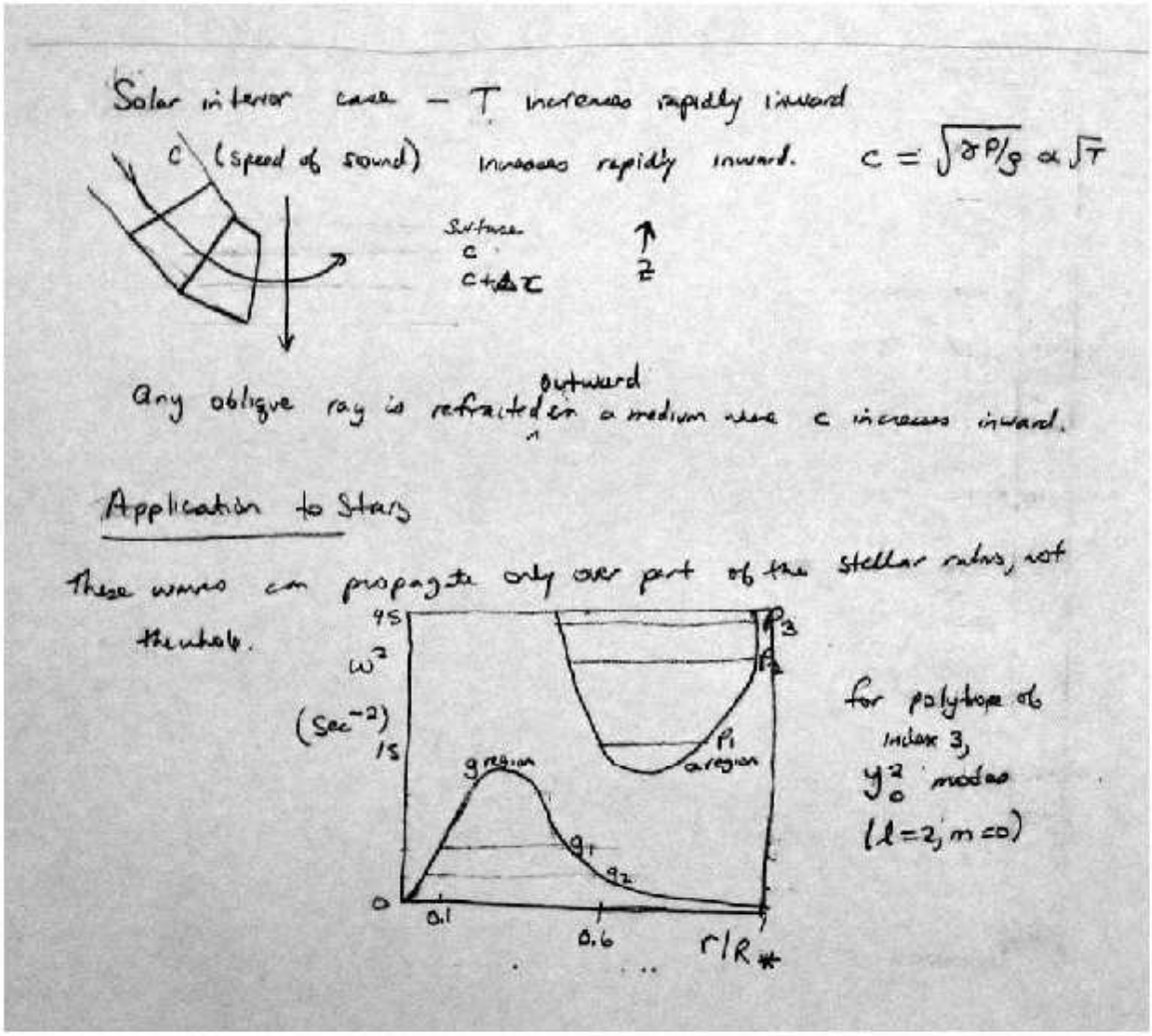

Fig. 2.— Refraction of a pressure wave due to sound speed increasing inward. Sketch of region in radius over which pressure and gravity waves propagate in the Sun.

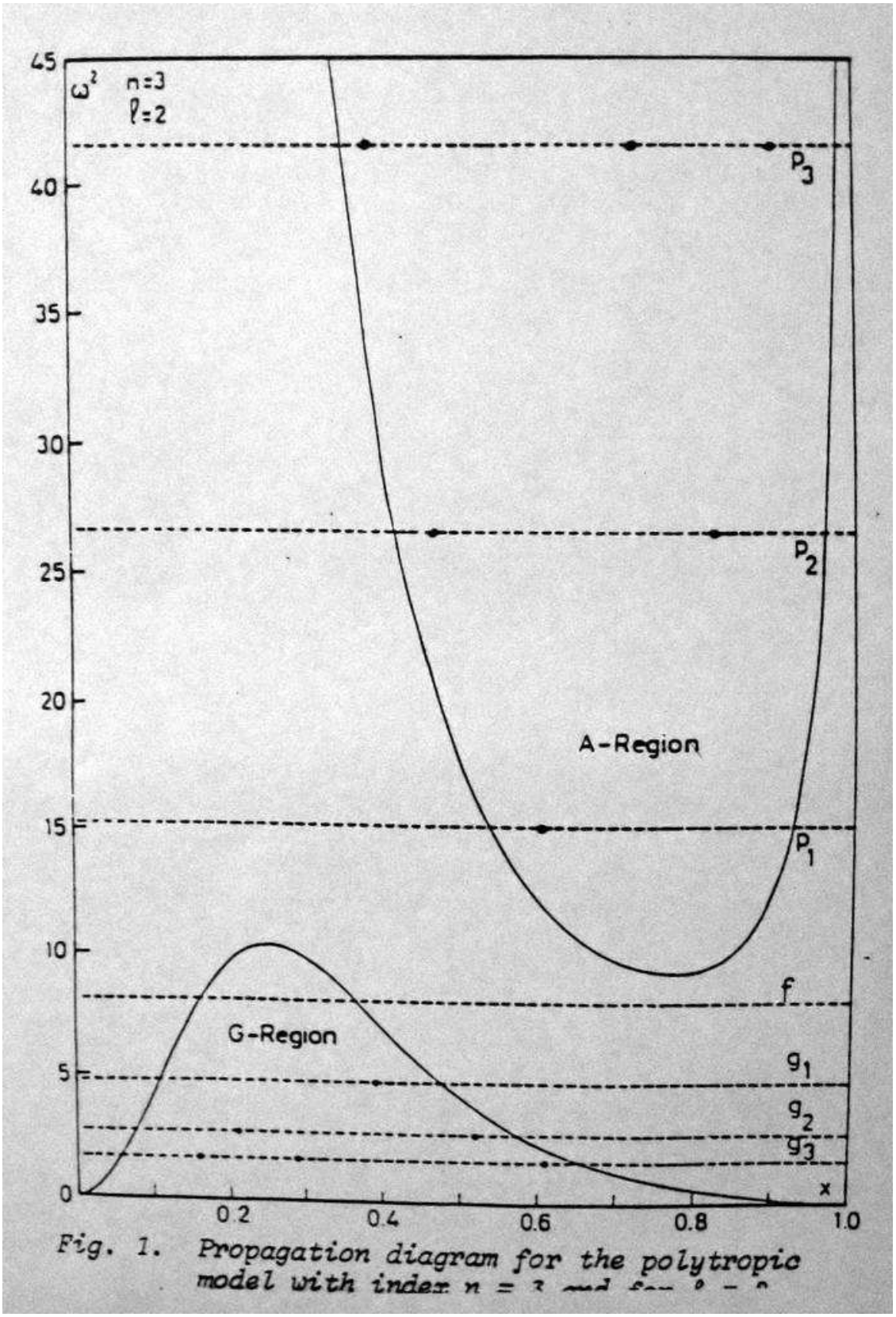

Fig. 1. Propagation diagram for the polytropic model with index n = 3 and for ℓ = 2

Fig. 3.— Pressure and gravity waves computed for a polytrope with $n = 3$ and $l = 2$. X-axis is r/R, Y-axis is ω^2.

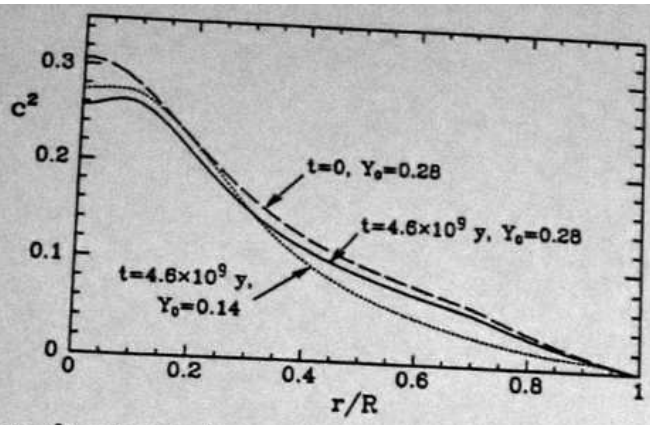

Figure 1 Square of sound speed, c^2, plotted against relative radius r/R in three solar models. The *continuous line* represents a standard model at the current time ($t = 4.6$ Gy) with $Z = 0.02$, $Y_0 = 0.28$; the *dotted line* represents an initially helium-deficient model ($Z = 0.004$, $Y_0 = 0.14$), also at the current time; the *dashed line* represents the model with $Z = 0.02$, $Y_0 = 0.28$ on the zero-age main sequence. The sound speed c is measured in Mm s^{-1}.

GOUGH & TOOMRE

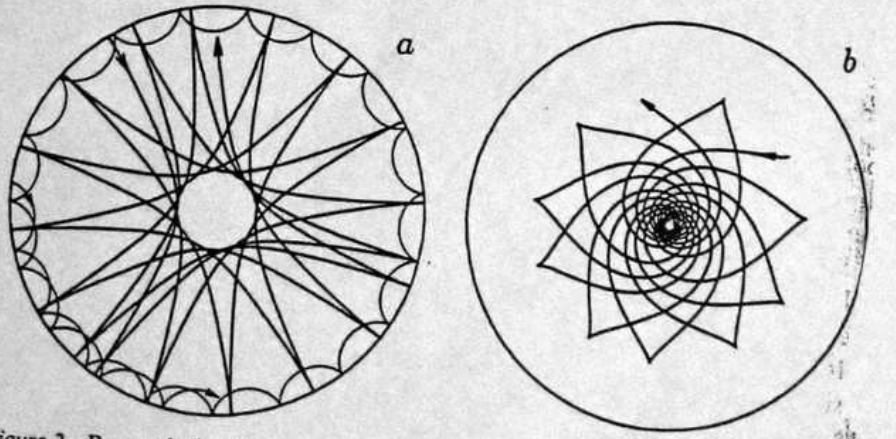

Figure 2 Ray paths in the standard model of the sun represented by the continuous line in Figure 1: (*a*) for two acoustic waves; the more deeply penetrating wave is p_8 ($l = 2$) and the shallower wave is p_8 ($l = 100$); (*b*) for the gravity wave g_{10} ($l = 5$). Note that the number of reflections per revolution is not integral, and indeed is almost never rational, so the ray paths are not closed.

Fig. 4.— Top: Square of sound speed is shown as a function of radius for 3 Solar models. Bottom: ray paths for several pressure and gravity modes.

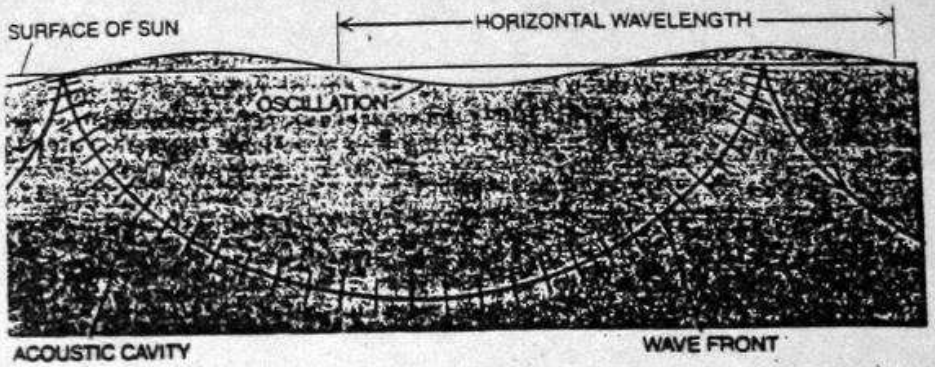

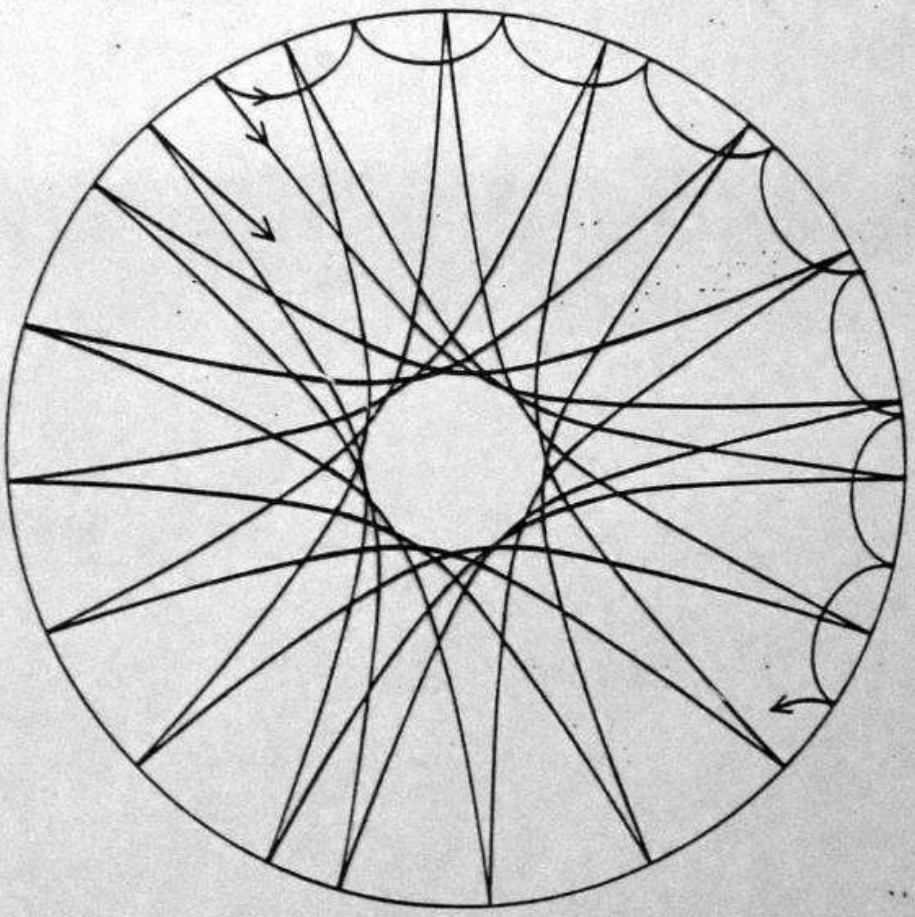

REFLECTION AND REFRACTION below the surface of the sun confine sound waves within acoustic cavities. A sound wave emerging from the solar interior is reflected by the steep decrease in density just below the surface (*top*); as the reflected wave descends it is refracted by the increase in the speed of sound with depth, which in effect rotates the wave fronts until they are again pointing toward the surface. Such trapped waves interfere constructively with themselves as they circle the sun, creating resonances that are detectable as oscillations of the solar surface. The horizontal wavelength and the period of the surface oscillation vary with the period of the wave that sets up the resonance and its depth of penetration. Penetration depth in turn depends on the orientation of the wave when it is reflected. As is shown in the cross section of the sun at the bottom, waves that travel steeply downward are refracted slowly and therefore probe the sun to a great depth; waves that penetrate at a more oblique angle are refracted more quickly and are confined to a shallower cavity.

53

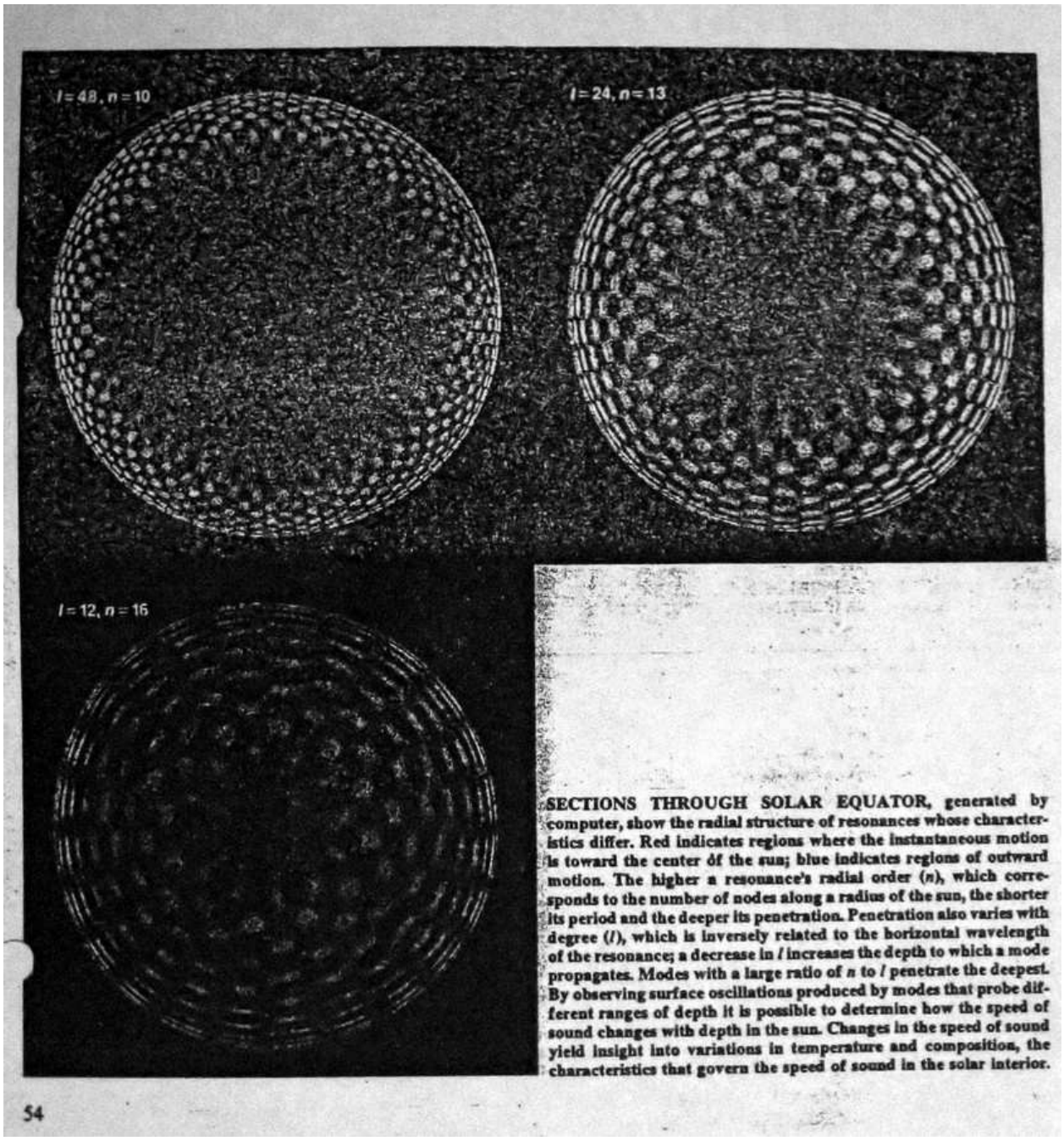

Fig. 5.— Illustration of high order modes.

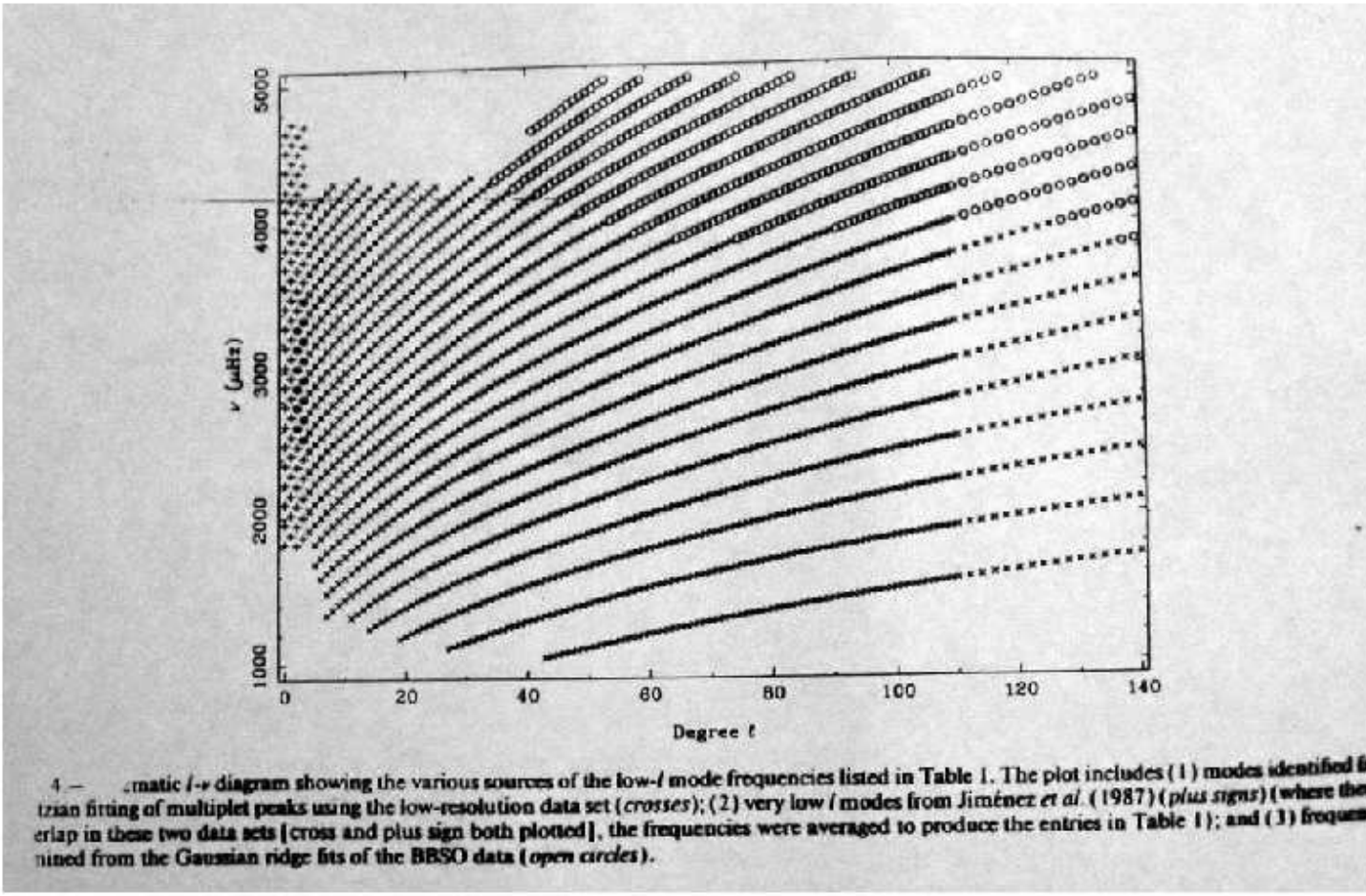

4 — matic l-ν diagram showing the various sources of the low-l mode frequencies listed in Table 1. The plot includes (1) modes identified f
tzian fitting of multiplet peaks using the low-resolution data set (*crosses*); (2) very low l modes from Jiménez *et al.* (1987) (*plus signs*) (where the
erlap in these two data sets [cross and plus sign both plotted], the frequencies were averaged to produce the entries in Table 1); and (3) frequen
ined from the Gaussian ridge fits of the BBSO data (*open circles*).

Fig. 6.— Observed pressure mode frequencies in the Sun as a function of horizontal wave number, from Libbrecht et al (1991).

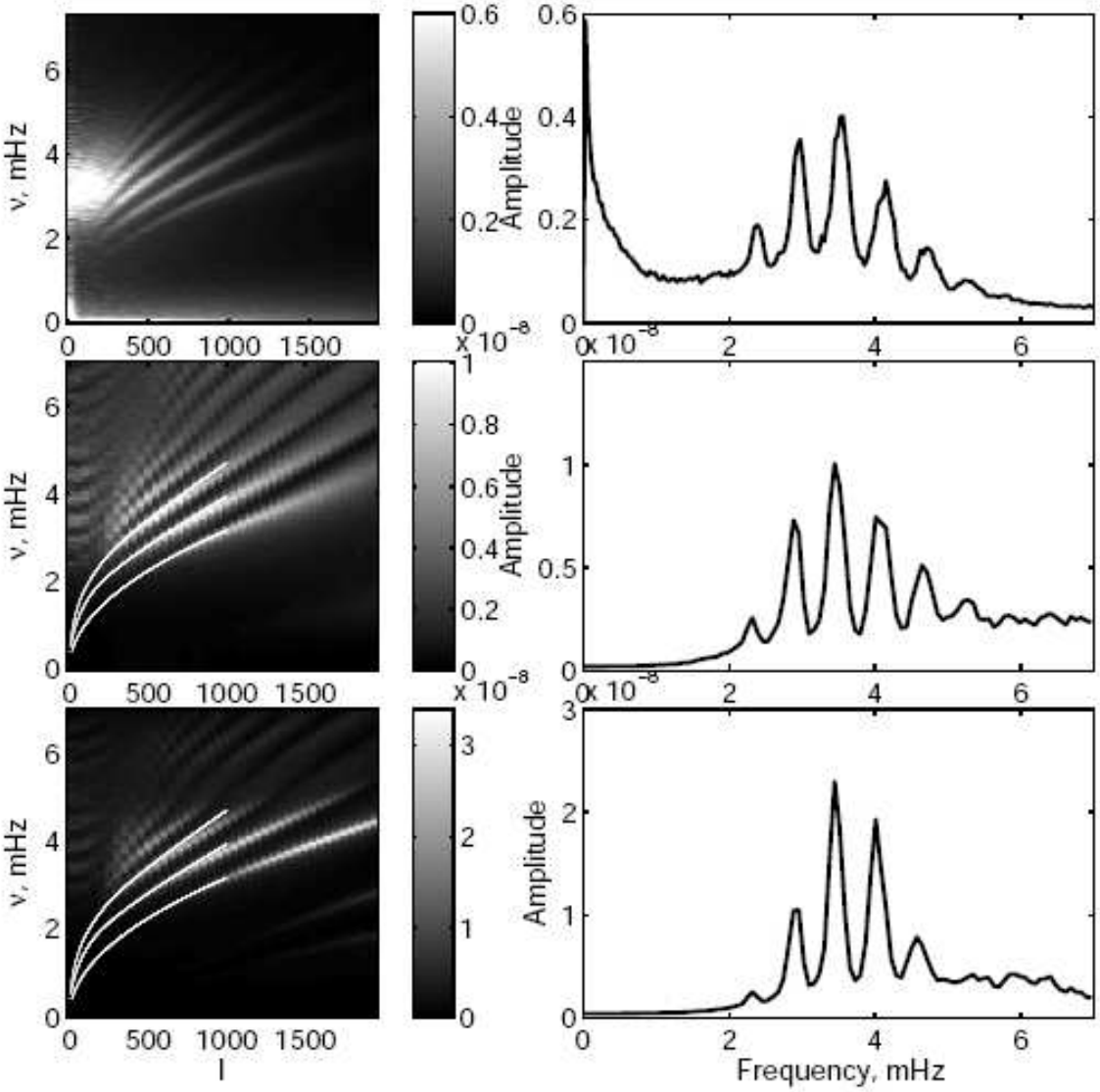

Fig. 9.— Acoustic spectra obtained from observations and simulations with different heights of the top boundary (the left panes). Starting from the top: observations, simulations with h_{top}=500 km, simulations with h_{top}=1750 km. The thin white curves on the left panes show position of observational ridges for f, p_1, and p_2 modes. The right panes show cuts of k-ω diagrams from left panes at l=584. For simulations with high top boundary without additional damping (bottom row) acoustic modes trapped in the domain distort the shape of the acoustic spectrum.

Fig. 7.— Observed amplitude of p-mode oscillations in the Sun as a function of frequency and comparison with models. (Fig. 9 from Parchevsky & Kosovichev, 2007, ApJ, 666, 547)

1.7. Uses of Helioseismology

The frequencies of the modes of solar oscillations can be measured to very high accuracy, at least 1 part in 10^5. This means that tests of fine details of a Solar model can be carried out by comparing the observed mode frequencies with those predicted from the model.

Parameters in the Solar model which can be studied are those which affect $c_s(r)$ or the mode splittings.

These tests probe the characteristics of the Sun well below the surface, one of the few methods, aside from studying Solar neutrinos, of obtaining any information about such deep layers.

Among the parameters that can be probed in this way are: the He content, the heavy element content Z, the depth of the top of the convection zone, and the mixing length for convection. The rotation as a function of depth can be inferred in this way, so that differential rotation both at the surface (studied from sunspot motions) and within the outer part of the Sun, can be measured. All these are for the outer layers of the Sun. Some information on the Solar core can also be obtained, in particular the rotation rate.

See the references for details.

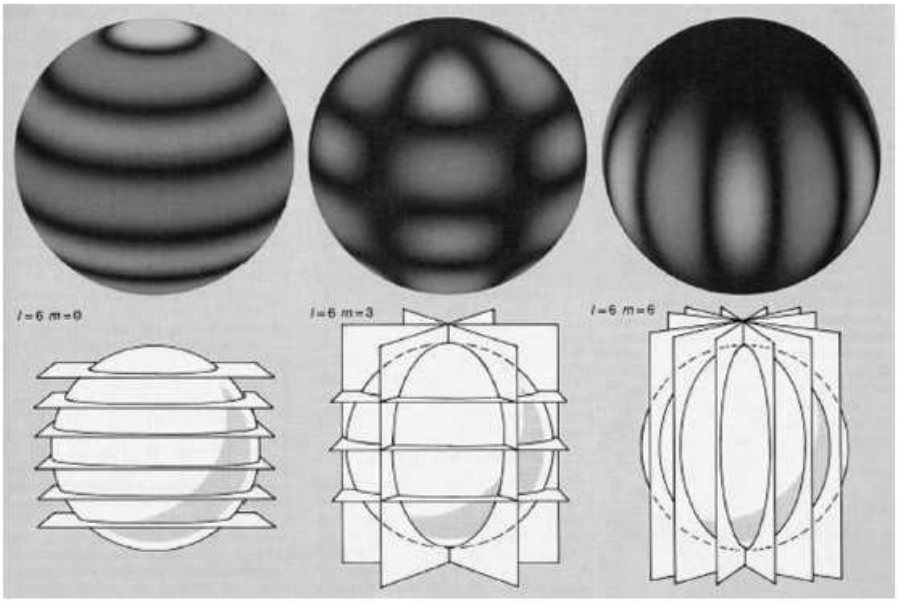

FIG. 1. Spherical harmonics for $l = 6$, $m = 0$, $m = 3$, and $m = 6$, respectively, from left to right (Courtesy J. W. Leibacher, National Solar Observatory).

Fig. 8.— Illustrative spherical harmonics (modes), from J. W. Leibacher, NSO, figure from Demarque & Guenther, 1999)

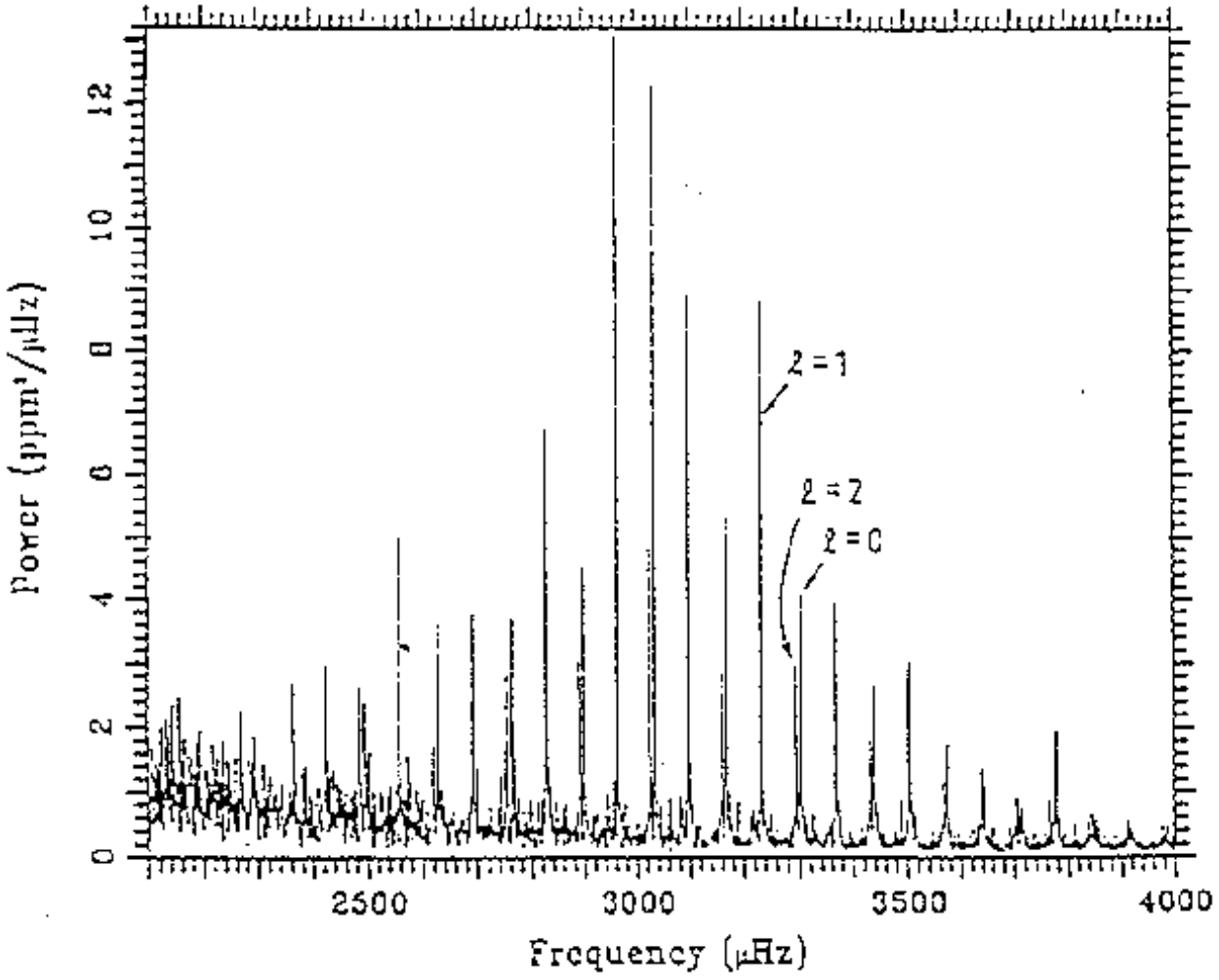

Fig. 9.— The splitting up of a solar mode. (From the COROT web site).

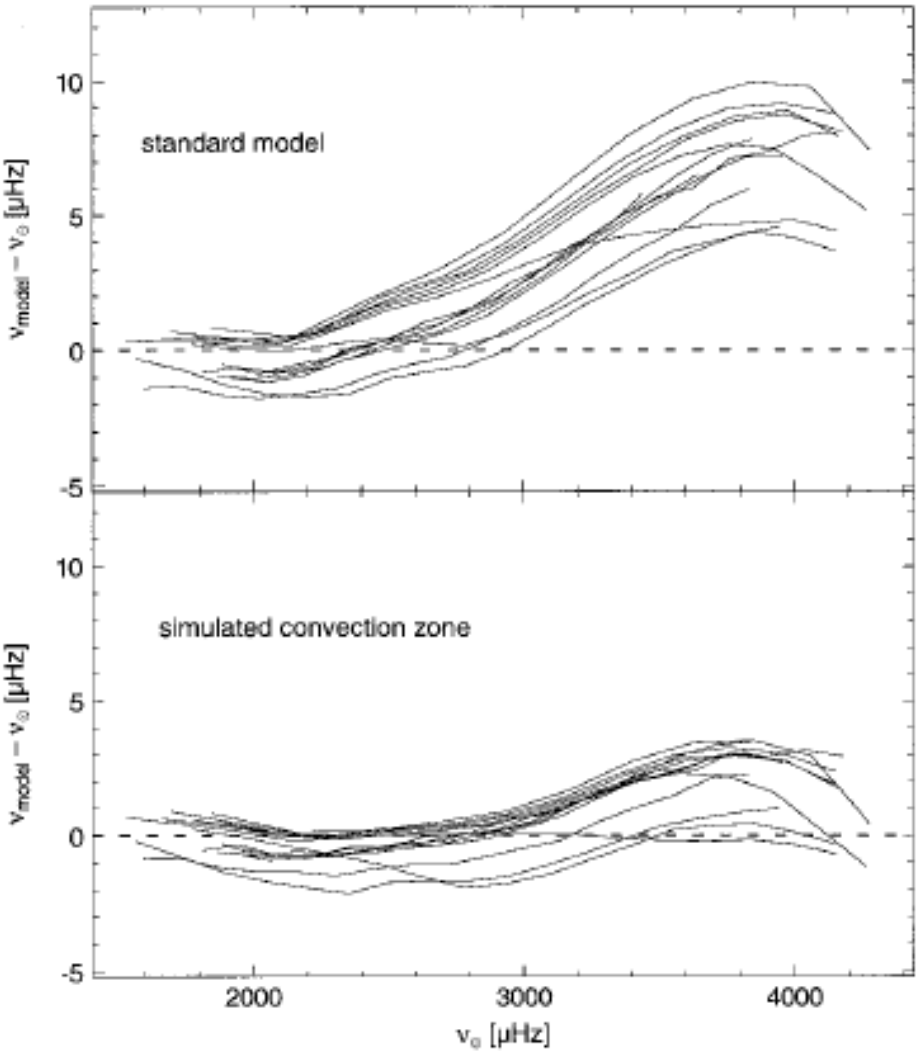

FIG. 5. Frequency difference diagrams (calculated minus observed) for solar p-modes with degree l in the range from 0 to 100. The upper panel shows a standard model constructed with the mixing length theory of convection, and the lower panel shows the same interior model with a more realistic simulated convection zone.

Fig. 10.— The difference between observed Solar p-mode frequencies and those predicted using various theories of convection. (from Demarque & Guenther, 1999)

2. Asteroseismology

The first major asteroseismology project was the Whole Earth Telescope set up by Don Winget of the University of Texas at Austin. This was a collaboration of people interested in asteroseismology at different observatories with small telescopes. The mode of operation was that they all joined in targeted photometric campaigns focused on a single star, each of which lasted for several months. They had 1 or two such joint campaigns per year.

Because one cannot resolve the surface of stars other than the Sun (except with interferometry, and there not in any detail), one can only hope to detect low order modes in other stars. These have been seen in many stars. The photometric precision with ground-based observations is not good enough to detect higher order modes in general. Such higher order modes largely cancel out in the integrated light across the surface of a star. The modes that are of highest amplitude in a particular star may vary with time and are not always the same.

Groups of stars pulsating in non-radial modes include stars similar to the Sun, PG 1159 stars (very hot hydrogen deficient post-AGB stars, with surface layers rich in He, C and O) (Vauclair et al, 2002), ZZ Ceti stars, and pulsating white dwarfs (see the appended HR diagram).

If a star is evolving very rapidly, then one may be able to measure the change in period with time for a particular pulsation mode. This provides a very useful check on stellar evolution and pulsational theory. Such a test has been carried out for a small number of compact stars with short period oscillations as well as for many Cepheid variables. (Cepheids are fundamental mode radial oscillators, a case to be discussed below.)

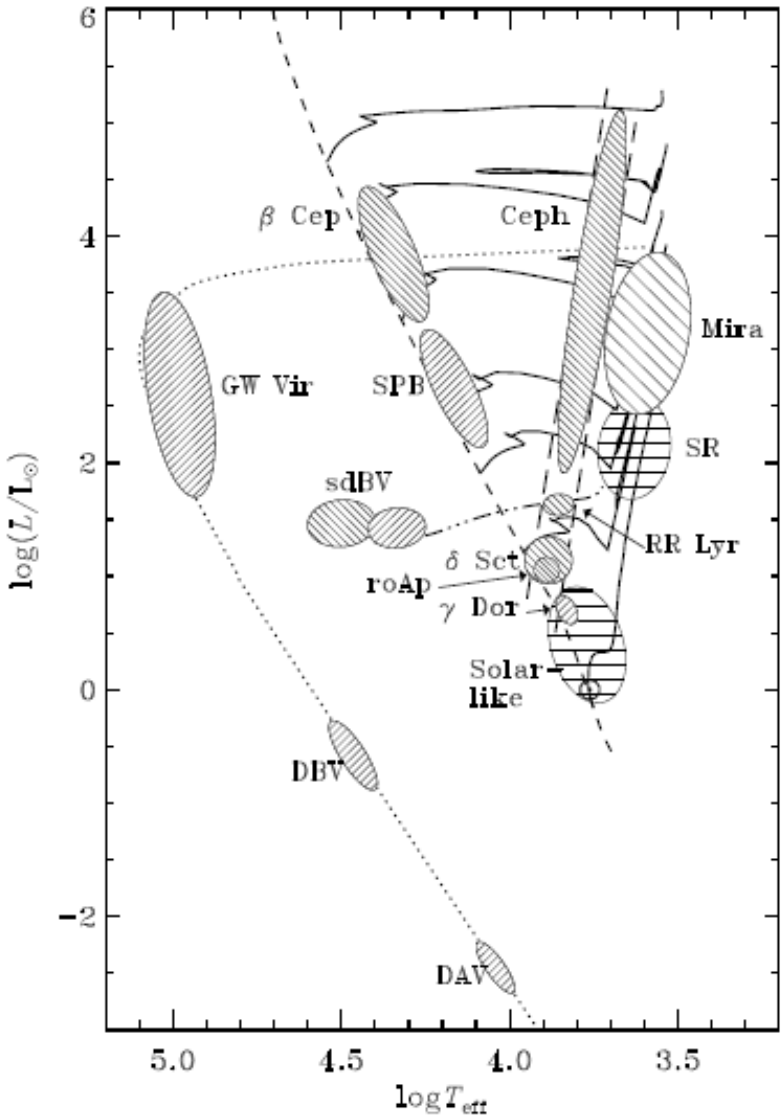

Fig. 1 Hertzsprung-Russell Diagram showing different classes of pulsating stars. Some of these are named after a particular member of the class. Others are acronyms, standing, respectively, for: rapidly oscillating Ap (roAp); Slowly Pulsating B (SPB); subdwarf B variables (sdBV). The group labelled GW Vir includes what has formerly been known as the PNNV stars (for Planetary Nebulae Nuclei Variables), and the variable hot DO white dwarfs (DOV); the DBV and DAV stars are variable DB (helium-rich) and DA (hydrogen-rich) white dwarfs. The parallel long-dashed lines indicate the Cepheid instability strip.

Fig. 11.— Figure by Christensen-Dalsgaard, taken from review by Cunha et al, Fig. 1 there)

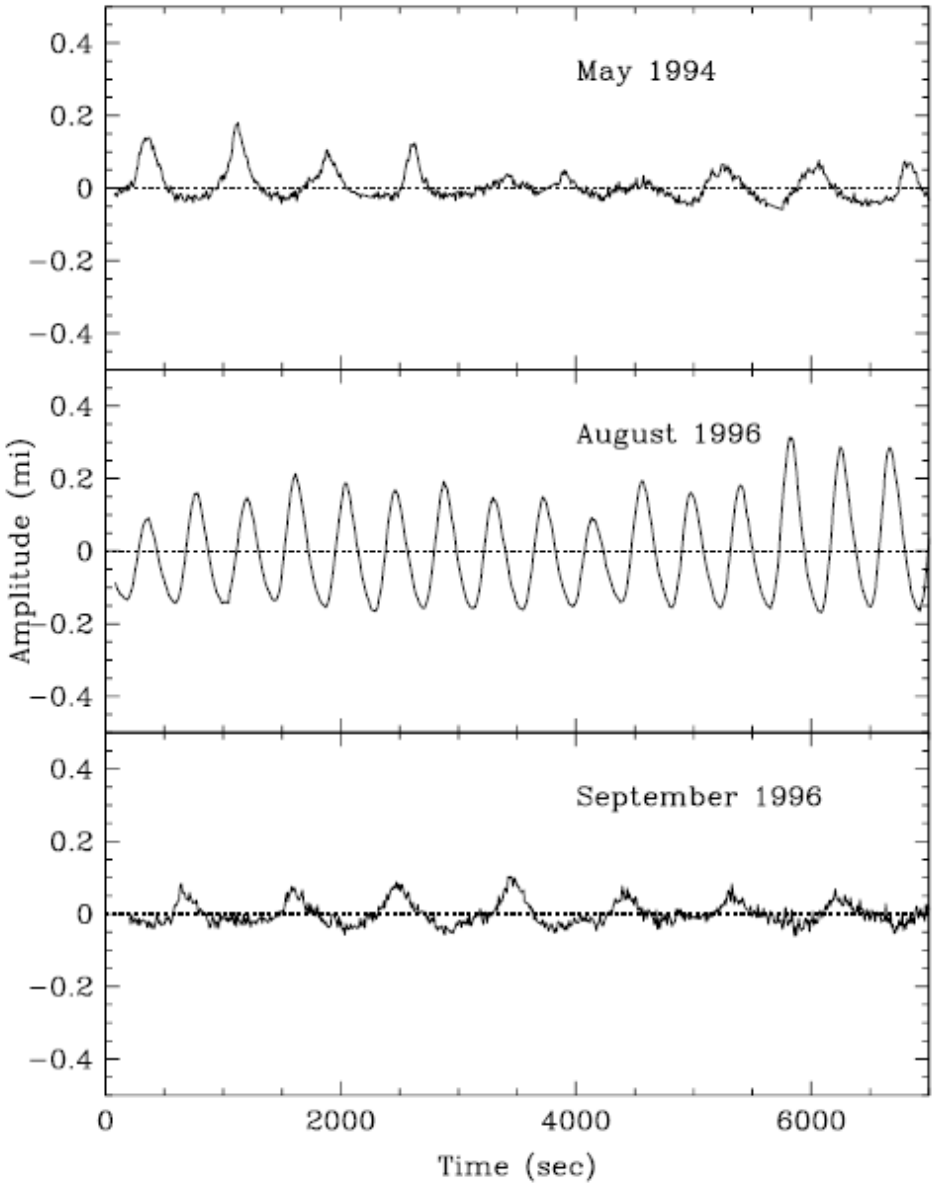

Fig. 8. GD 358 lightcurves over time. The shape of the lightcurve was sinusoidal when the amplitude was highest. The 1994 and September 1996 data exhibit similar pulse shapes and their corresponding power spectra also look similar

Fig. 12.— The light curve of the pulsating white dwarf GC 358 at three different epochs. The vertical scale is mag. (From the WET, Kepler et al. 2003)

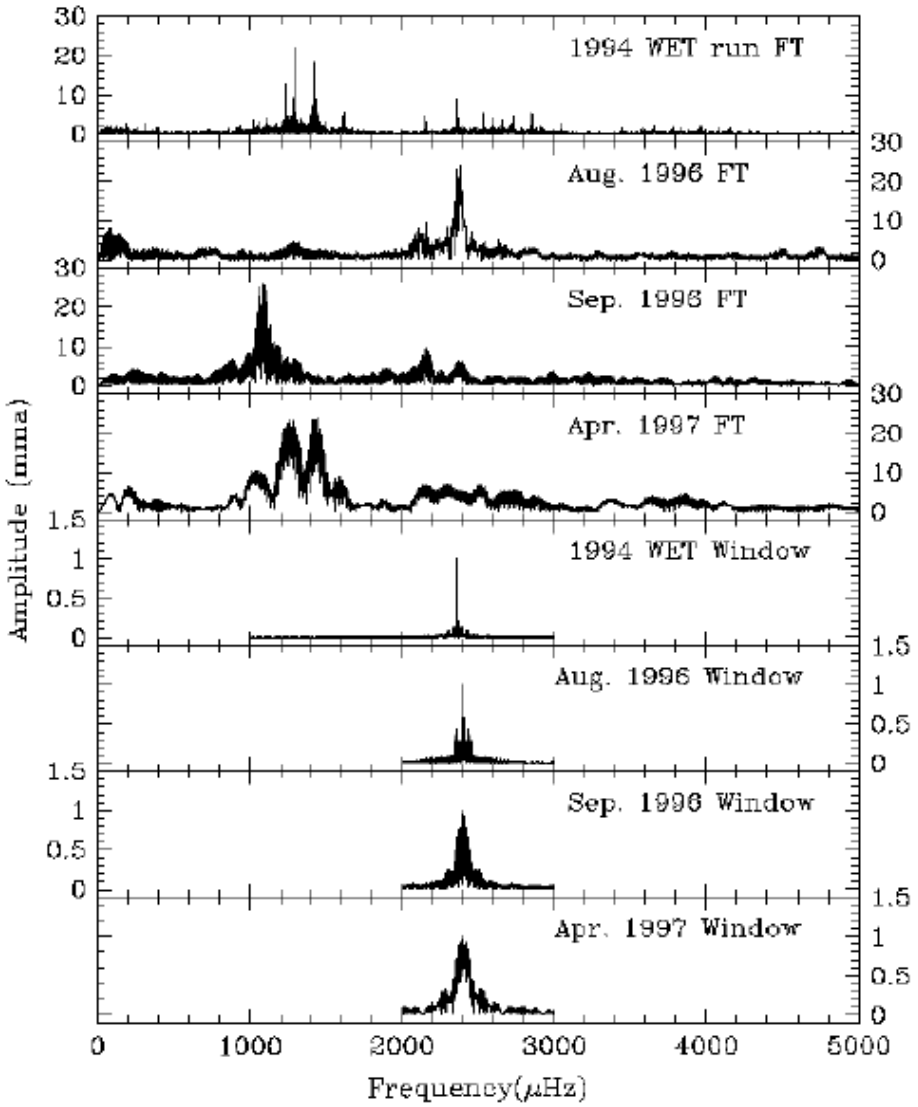

Fig. 7. GD 358 Fourier transform at four different times along with their spectral windows. The 1994 and 1997 Fourier transforms look similar (within the observed frequency resolution, that is). The September 1996 data look similar as well to these two data sets, but the highest amplitude modes have shorter frequencies (longer period). Obviously, the August 1996 Fourier transform looks very different from the other Fourier transforms.

Fig. 13.— The power spectrum for photometry of GD 358 at different epochs. (From the WET, Kepler et al. 2003)

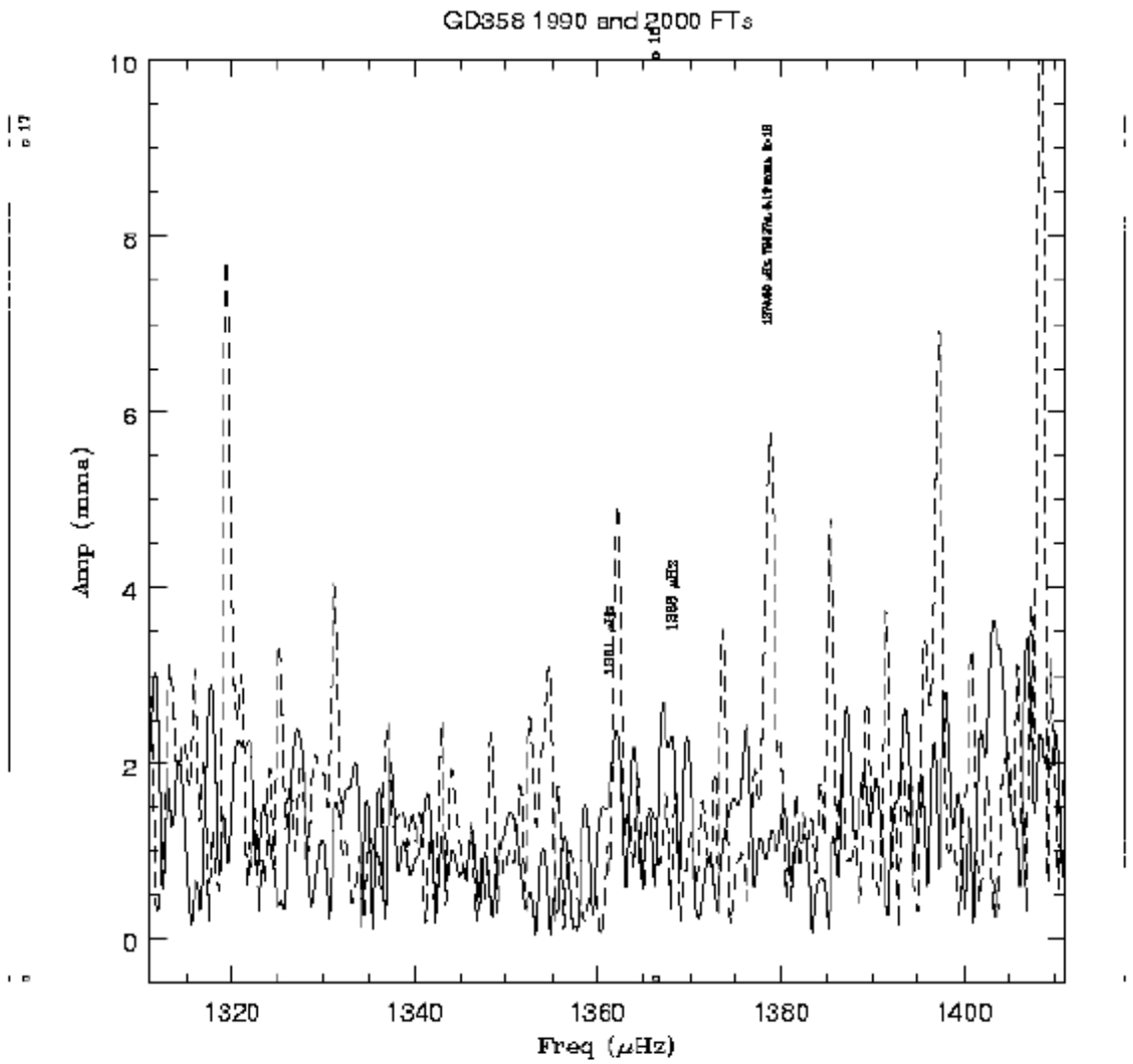

Fig. 11. Peaks around k=16 in the 1990 (solid line) and 2000 (dashed line) transforms

Fig. 14.— Details of some of the modes present in GD 358, a pulsating white dwarf, around $k = 16$ at two epochs four years apart. (From the WET, Kepler et al. 2003)

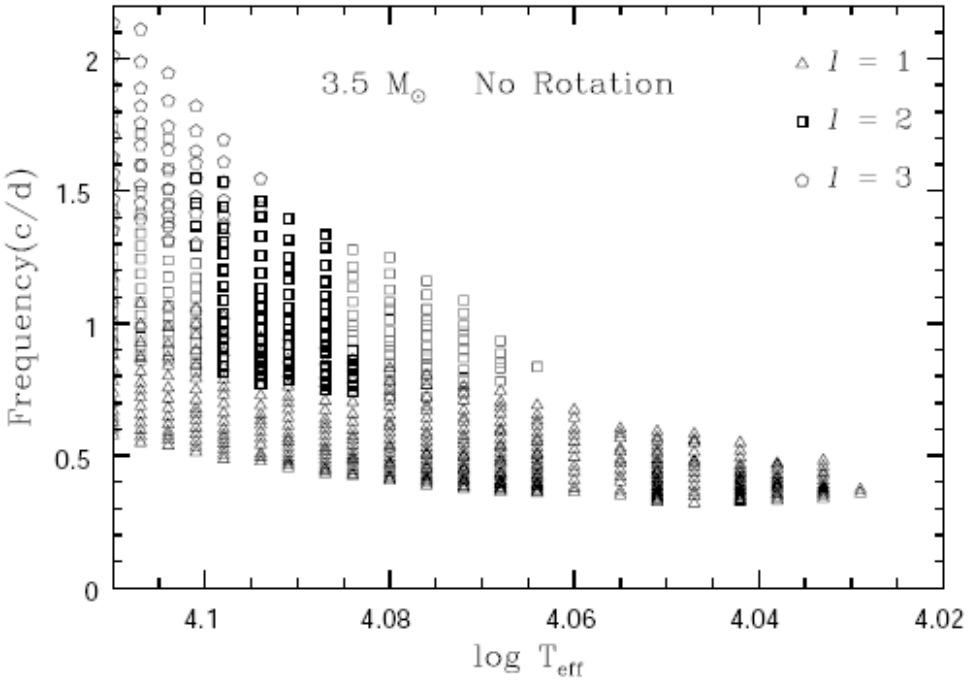

Fig. 4.— Frequencies of g-modes excited in non-rotating models along the $3.5M_{\odot}$ main-sequence evolution. The evolutionary track is shown in Fig. 3.

Fig. 15.— Predicted frequencies (cycles/day) of the g-modes for the late type main sequence Be star β CMi (B8Ve) as it evolves off the main sequence from T_{eff} 12,900 K to 10,500 K. (From Saio, Cameron, Kuschnig et al, 2007)

3. Radial Modes

We now repeat our earlier derivation for eigenfunctions and their frequencies using spherical coordinates to search for the radial modes. We need the same three equations described earlier. We use the same notation as before, so that for example ρ^1 is the (small) change in density as compared to the initial equilibrium value ρ_0. We again assume adiabatic conditions for the moving parcel of gas. Thus equation 2 is the same as before, and is derived from $P \propto \rho^\gamma$. Its perturbed form is also identical to equation IIp given earlier.

Equation 1 (mass conservation) is now

$$\frac{\partial M_r}{\partial r} \;=\; 4\pi r^2 \rho \quad (eq.\ I\ radial)$$

To obtain the perturbed form of this equation, we note that the left side becomes

$$\frac{\partial M_r}{\partial r} \;=\; \frac{\partial M_r}{\partial [r_0(1 + r^1/r_0)]}$$

The perturbed form of this equation is

$$\frac{\rho^1}{\rho_o} \;=\; -\,3\frac{r^1}{r_0} \;-\; r_o\,\frac{\partial (r^1/r_0)}{\partial r_0} \quad (eq.\ Ip - radial)$$

The force equation for the radial case is HKT eq. 8.2,

$$\frac{d^2 r}{dt^2} \;=\; -\;4\pi r^2\,\frac{\partial P}{\partial M_r} \;-\; \frac{GM_r}{r^2} \quad (eq.\ III\ radial),$$

with the perturbed version being HKT eq. 8.7.

Through substitution and differentiation, in a manner similar to what we did earlier to derive the speed of sound, we construct the linearized adiabatic wave equation (LAWE). Details are given § 8.1 of HKT. We then look for sinusoidal solutions, separating the radial and time dependence,

$$\frac{r^1(t, r_0)}{r_0} \;=\; \frac{r^1(r_0)}{r_0}\; e^{i\sigma t}$$

where σ may turn out to be complex; if it is real, $\sigma = \omega$.

The LAWE is difficult to solve. We consider for illustrative purposes a simpler case, setting the wave amplitude independent of r. We then find, for the constant density model,

$$(3\gamma - 4)\; \frac{4\pi G}{3}\; <\rho> \;\;=\;\; \sigma^2.$$

If $\gamma > 4/3$, σ is real, and the corresponding period Π is

$$\Pi \;=\; 2\pi/\sigma \;=\; \frac{2\pi}{\sqrt{(3\gamma - 4)\;\; <\rho> \;\; 4\pi G/3}}$$

If $\gamma < 4/3$, the perturbation either grows or decays exponentially. This does not correspond to radial pulsations; the "period" is the approximately the free fall time (the dynamical timescale).

For the radial modes, the stellar surface swells and contracts, the surface temperature and emitted flux change over the period, and the amplitude of variation observed is much larger than for the small amplitude non-radial modes seen in the Sun. The overtones do not have a node at the surface either. (Fig.-8.1 of HKT shows the radial displacements as a function of r/R calculated for the fundamental and first two overtone modes in a $n = 2$ polytrope).

The stars we normally consider variable stars (Cepheids, RR Lyraes, etc) are radially pulsating stars.

Our dispersion relation for pressure waves is $(\omega^2 - \omega_c^2) = c_s^2 k_z^2$ for the constant temperature case. For $\omega^2 >> \omega_c^2$, we have $\omega^2 = c_s^2 k_z^2$. The fundamental mode has $\lambda = 4R$ and $k_z = 2\pi/(4R)$.

Since $c_s^2 = \gamma P_0/\rho_0$, the period of the mode Π is then

$$\Pi \;=\; \frac{2\pi}{\omega} \;=\; 4R\sqrt{\frac{\rho_0}{\gamma P_0}}.$$

We use the equation of hydrostatic equilibrium in its approximate form

$$\frac{dP}{dr} \;=\; -\rho g \;=\; -\rho\, G\, \frac{M}{R^2} \;\approx\; \frac{< P >}{R}.$$

So $< \rho > / < P >= R/GM$, and hence the (approximate) constant Q is defined as

$$Q \;=\; \Pi\sqrt{\frac{< \rho >}{< \rho_\odot >}}.$$

Doing this more carefully, one obtains

$$\Pi \;=\; \sqrt{\frac{3\pi}{(3\gamma - 4)\; G \;< \rho >}}$$

Inserting the value of Q for the Sun, we find for the fundamental radial mode of pulsation:

$$\Pi \;=\; 0.04\,\sqrt{\frac{< \rho_\odot >}{< \rho >}}\ \text{days}$$

Since the mean density of stars varies enormously from $10^6 > \frac{<\rho>}{<\rho_\odot>} > 10^{-9}$ there is an enormous range in the period of the fundamental mode of pulsation, from 3 sec to 1000 days. Harmonics have smaller λ, larger k_z, and shorter periods. In all cases, the surface $r = R$ is not anode of the motion. The range in Q from observations of variable stars is much smaller, 0.02 to 0.12 days.

For the isothermal atmosphere discussed above, we find that the oscillation eigenvalue is proportional to $e^{z/H}\ e^{i(\omega t - k_x x - k_z z)}$. (By symmetry we do not need to consider the third axis, i.e. we use k_x here instead of $\sqrt{k_x^2 + k_y^2}$, ignoring rotation, magnetic fields, etc. which would distinguish the k_x and k_y terms.) Since the pressure scale height $H = P_0/(\rho_0 g)$, the amplitude of the oscillation decreases as the temperature increases. Thus the largest amplitude is near the surface. The amplitude in the core is decreased by the very large ratio of $\rho(core)/\rho(surface)$. We can thus ignore any pulsations in the core, and this implies that variations in the nuclear energy generation rate ϵ cannot drive pulsations.

MOST photometry of the RRd Lyrae variable AQ Leo

Table 1. Frequencies identified in AQ Leo from the MOST photometry by Sig8pec, which are consistent with the other frequ analysis techniques described in the text. Amplitudes, phases, significances, and uncertainties (derived by bootstrapping) are also li The phases correspond to epoch JD2000 = JD2451545.

id: identification, *f:* frequency [d^{-1}], σ_f*:* error in frequency [d^{-1}] (1σ), *A:* amplitude [mmag], σ_A*:* error in amplitude [mmag] (1σ), spectral significance, θ*:* phase, σ_θ*:* error in phase (1σ), *comb.err.:* deviation $f - f_c$ from the numerical value for combinations $f_c = af_0 + bf_1 + cf_i$

	id		f	σ_f	A	σ_A	sig.	θ	σ_θ	comb.err.
–	f_1	–	2.43821	0.00001	204.3	0.106	11982	−1.855	0.001	0.00000
–	$2f_1$	–	4.87673	0.00004	46.4	0.102	5931	1.246	0.005	0.00031
–	$3f_1$	–	7.31515	0.00013	16.6	0.101	2502	−2.417	0.014	0.00052
–	$4f_1$	–	9.75228	0.00064	5.4	0.118	521	−2.855	0.069	−0.00056
–	$5f_1$	–	12.18890	0.00188	0.8	0.103	16	2.344	0.141	−0.00215
f_0	–	–	1.81896	0.00002	113.5	0.098	10702	1.612	0.002	0.00000
$2f_0$	–	–	3.63822	0.00019	16.3	0.105	2780	2.777	0.022	0.00030
$3f_0$	–	–	5.45637	0.00098	3.3	0.120	203	2.703	0.113	−0.00051
f_0	f_1	–	4.25723	0.00004	50.1	0.099	5001	2.596	0.005	0.00006
$-f_0$	f_1	–	0.61923	0.00005	45.5	0.120	8321	−1.097	0.006	−0.00002
f_0	$2f_1$	–	6.69543	0.00010	21.0	0.104	3268	2.507	0.011	0.00005
$-f_0$	$2f_1$	–	3.05758	0.00034	10.6	0.108	1392	1.245	0.038	0.00012
f_0	$3f_1$	–	9.13385	0.00025	9.0	0.103	1304	−2.346	0.028	0.00026
$-f_0$	$3f_1$	–	5.49405	0.00288	1.3	0.115	38	1.066	0.305	−0.00162
f_0	$4f_1$	–	11.56975	0.00053	3.9	0.105	275	1.323	0.059	−0.00205
$-f_0$	$4f_1$	–	7.93297	0.00103	2.3	0.115	104	−2.354	0.129	−0.00091
$-f_0$	$5f_1$	–	10.37055	0.00225	1.2	0.104	32	3.033	0.210	−0.00154
$2f_0$	f_1	–	6.07720	0.00021	10.6	0.102	1503	−0.727	0.025	0.00107
$2f_0$	$-f_1$	–	1.19802	0.00039	5.9	0.107	604	2.930	0.048	−0.00169
$2f_0$	$2f_1$	–	8.51455	0.00023	10.5	0.103	1606	1.244	0.024	0.00021
$-2f_0$	$2f_1$	–	1.23813	0.00087	2.9	0.105	161	2.125	0.102	−0.00037
$2f_0$	$3f_1$	–	10.95270	0.00099	3.3	0.104	203	−0.148	0.114	0.00015
$-2f_0$	$3f_1$	–	3.67725	0.00114	2.8	0.108	152	1.295	0.133	0.00054
$2f_0$	$4f_1$	–	13.38950	0.00097	1.8	0.105	67	1.820	0.120	−0.00126
$-2f_0$	$4f_1$	–	6.12023	0.00137	1.7	0.106	57	1.765	0.148	0.00531
$2f_0$	$5f_1$	–	15.82902	0.00170	1.1	0.103	26	−2.082	0.179	0.00005
$-2f_0$	$5f_1$	–	8.55350	0.00189	1.3	0.101	34	0.463	0.209	0.00037
$-2f_0$	$6f_1$	–	10.99215	0.00366	0.9	0.101	19	−0.578	0.322	0.00081
$3f_0$	f_1	–	7.89427	0.00093	3.0	0.113	173	−0.447	0.117	−0.00082
$3f_0$	$2f_1$	–	10.33075	0.00155	1.8	0.104	68	2.806	0.168	−0.00255
$3f_0$	$3f_1$	–	12.77310	0.00410	0.7	0.102	11	2.485	0.272	0.00159
$4f_0$	f_1	–	9.71217	0.00329	0.9	0.117	17	1.952	0.351	−0.00188
–	–	f_i	1.96161	0.00257	1.6	0.100	53	1.114	0.381	0.00000
–	f_1	f_i	4.40172	0.00229	0.8	0.100	14	−0.942	0.292	0.00190
–	–	$2f_i = f_{ii}$	3.92593	0.00144	2.5	0.117	122	2.014	0.117	0.00271
–	f_1	$2f_i$	6.36320	0.00240	1.0	0.109	23	−2.042	0.216	0.00177
$f0$	f_1	$2f_i$	8.18505	0.00246	0.7	0.103	11	−2.445	0.289	0.00466
$-3f0$	$3f_1$	$2f_i$	5.78067	0.00238	0.8	0.101	16	−1.855	0.319	−0.00030
$-4f0$	$2f_1$	$2f_i$	1.52777	0.00382	0.8	0.101	13	−1.957	0.248	0.00397
$-4f0$	$3f_1$	$2f_i$	3.95930	0.00167	1.4	0.124	40	−2.055	0.136	−0.00271
$-4f0$	$4f_1$	$2f_i$	6.39875	0.00193	1.4	0.109	43	0.931	0.169	−0.00147
$-4f0$	$5f_1$	$2f_i$	8.83928	0.00445	0.8	0.101	15	−2.741	0.632	0.00085

Fig. 16.— Table of the modes present in the light curve of AQ Leo, a RR Lyrae star, from observations with the MOST satellite. There are 2 main modes, the fundamental and the first overtone radial modes, with $f = 2.438$ and 1.819 cycles/day, plus various combinations of sums and differences of these. The last few modes in the table may be spurious and result from aliases or instrumental issues. (From Gruberbauer et al, 2007)

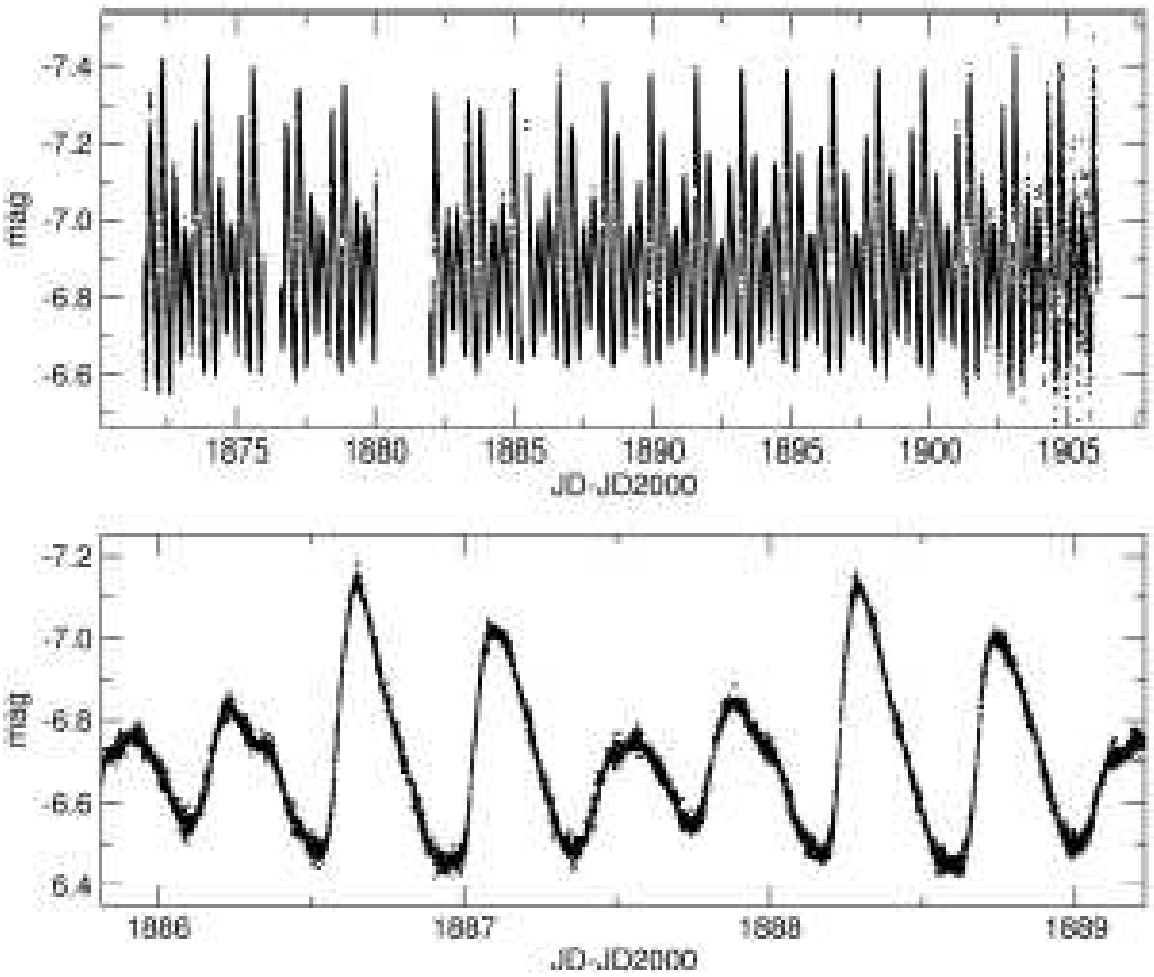

Figure 1. The light curve of AQ Leo obtained by MOST. The entire time series (upper panel), as well as an expanded view of 3.7 days of the light curve (lower panel).

Fig. 17.— Light curve of AQ Leo, a RR Lyrae star, from the MOST satellite. (From Gruberbauer et al, 2007)

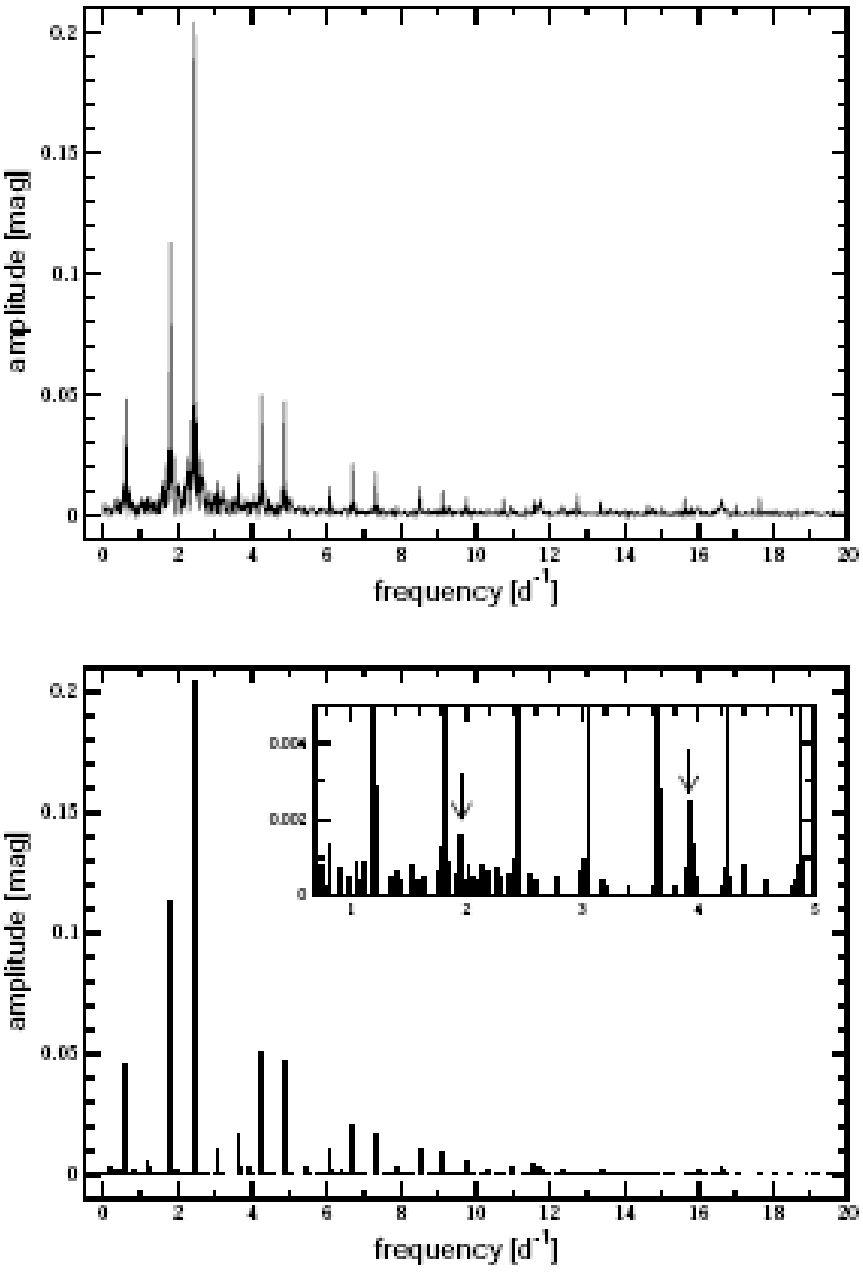

Figure 2. *Upper panel* : The amplitude spectrum of the AQ Leo light curve. Most of the linear combinations of f_0 and f_1 can be identified by eye. *Lower Panel* : The amplitude spectrum for frequencies identified by SigSpec. The inset is a close-up of the low frequency range containing f_4 and f_{11}.

Fig. 18.— The amplitude of various modes present in the light curve of AQ Leo, a RR Lyrae star. (From Gruberbauer et al, 2007)

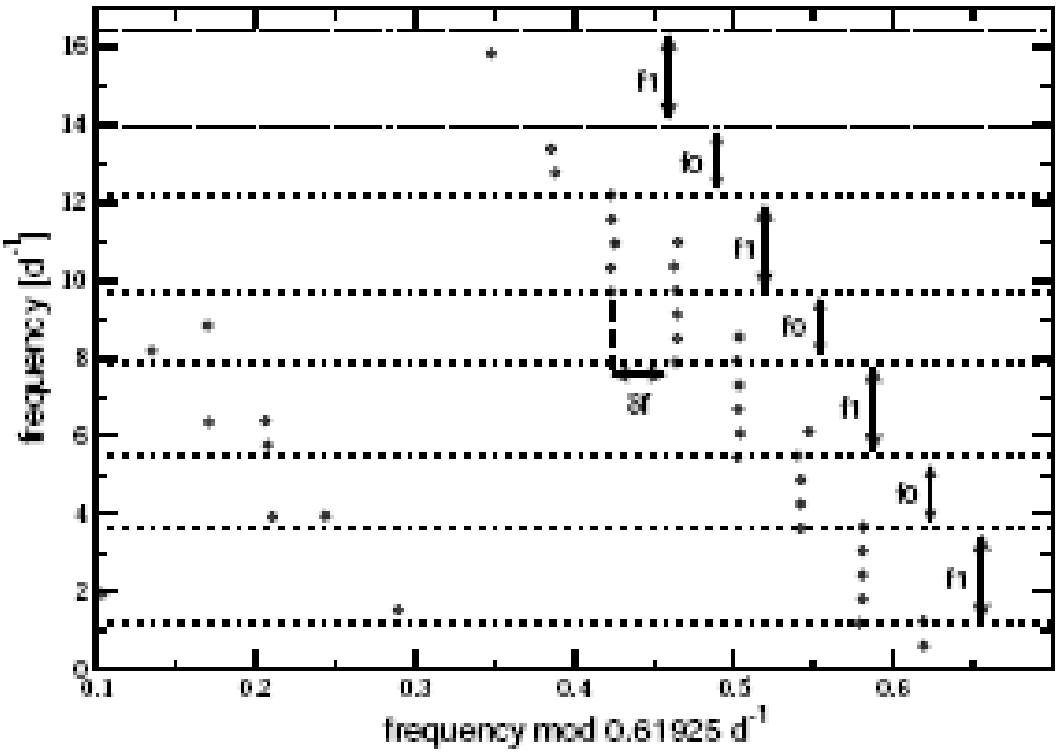

Figure 3. Graphical presentations of the linear combinations of the two dominant modes in AQ Leo, in the form of "echelle" diagrams. The observed frequencies folded at the beat frequency $f_1 - f_0 = 0.61925$ d^{-1} show differences of $\delta f = 3 \cdot f_1 - 4 \cdot f_0$ in a regular pattern alternating by f_0 and f_1.

Fig. 19.— Diagram of the modes present in AQ Leo, a RR Lyrae variable, from the MOST satellite. (From Gruberbauer et al, 2007)

4. Wave Excitation

Stellar pulsation is a long term phenomena; the pulsations are stable and persist over many cycles. Pulsations begin if/when the star is unstable for small displacements of a parcel of gas. There is always some small random $\delta P = P - P_0$ present. Pulsations grow in amplitude until non-linear effects limit the growth to the observed finite amplitudes. Pulsations die out when a star evolves into a configuration that is stable against pulsations. On such a very long timescale, pulsations are transient phenomena.

Energy must be fed into the pulsations via some driving mechanism to sustain them. Over most of the interior of the star, energy is lost during each pulsation cycle, and this effectively damps the pulsation. But in some radial regions, there must be energy fed into the pulsation, enough to overcome the effect of all the damping from other regions, for the pulsation to persist.

Consider the angular frequency $\omega = \omega_1 + i\omega_2$ where ω_1 and ω_2 are both real. A star will be pulsationally unstable if $\omega_2 < 0$, while if $\omega_2 > 0$ the mode displacement is proportional to $exp(- \mid \omega_2 \mid t)$, and the pulsation dies out exponentially.

A second requirement is that the pulsation becomes established on a timescale which is less than the evolutionary timescale of the star, $\sim 10^9$ yr for main sequence stars, smaller for more evolved stars.

To evaluate ω_2 requires using a non-adiabatic energy equation instead of assuming adiabatic motions of the gas. This is very difficult, see Cox & Guili §27 for a discussion. One finds that the existence of instability is related to the position of envelope ionization zones, often of He II, as that often falls in about the right temperature and radius of the star.

To evaluate this, we must consider the work done by the gas element as it expands and

then contracts. dQ, the work done on the element (i.e. the heat added to the parcel of gas) is $dU + dW$, where dW is the work done by the parcel of gas on its surroundings. Over the cycle, the integral of dU must be 0 since the beginning and end state are identical. A region which gains heat during the compression part of the cycle drives the pulsation, while regions that lose heat during the compression damp the pulsation.

W is the work done by the gas during the cycle, $W = \oint dQ$. Work is available to drive the oscillation if $\oint dQ > 0$. Since the entropy S is constant, $\oint dS = 0 = \oint dQ/T$. (Note that if T is constant throughout the cycle, $\oint dQ = 0 = W$ and there cannot be pulsations.)

Image $T(t)$ has a cyclic modulation, $T(t) = T_0 + \Delta T(t)$.

$$0 \;=\; \oint \frac{dQ(t)}{T_0 + \Delta T(t)} \;\approx\; \oint \frac{dQ(t)}{T_0}(1 - \Delta T/T_0)$$

Then

$$W \;=\; \oint dQ(t) \;=\; \oint dQ(t)\frac{\Delta T(t)}{T_0}$$

To have $W > 0$ integrated over a cycle requires that ΔT is positive when $dQ(t)$ is positive (heat is added to the element when the temperature is higher) and ΔT is negative when $dQ(t)$ is negative (heat is lose from the parcel of gas when T is low).

A star can pulsate if

$$W(total) \;=\; \int_0^M [\oint \frac{\Delta T}{T_0(m)}\, dQ(m)]\, dm \;>\; 0.$$

A careful study of this integral (the original early work is by Epstein, 1950, ApJ, 112, 6) suggests that the region of highest weight in the integral is at $r \sim 0.7R$.

Nuclear reaction rates behave to drive pulsations, ϵ increases rapidly when T increases, and the sign is correct for $W > 0$. However, as indicated above the pulsational amplitudes are very low in the stellar core and the integral over the nuclear burning regions is not big enough to overcome what may be happening in the outer parts of the star.

For most large amplitude pulsating stars, including all radial pulsators, the driving mechanism is related to the opacity, hence called the κ-mechanism. For this to work, the opacity must be large, thus usually from H or He. If one has an opacity κ such that κ increases when the star contracts, energy can be removed from the radiative flux at the proper time to drive oscillations. One can show that a radial zone with no nuclear energy generation is stable if

$$f(m) \; = \; \frac{4}{c} \; - \; (\frac{\kappa_T}{c} \; + \; \kappa_P) \; - \; \frac{4}{3\gamma} \; > \; 0, \quad \kappa_T \; = \; \frac{\partial ln\kappa}{\partial lnT}|_P \quad \text{and } \kappa_P \; = \; \frac{\partial ln\kappa}{\partial lnP}|_T,$$

and γ is the adiabatic index from $P \propto \rho^\gamma$. c here is from another adiabatic index, $PT^{\gamma_2/(1-\gamma_2)} =$ constant, and $\gamma_2 = c/(c-1)$. γ and c (from γ_2) are evaluated for adiabatic changes.

$4/c$ is always positive, so always promotes stability, but the opacity derivitives can be destabilizing if κ_T and/or κ_P are positive. The last term is always destabilizing (it arises from the spherical geometry). If the integral of $f(m)$ over the mass of the star is positive, the star is stable against pulsation.

We recall that in ionization zones, all of the adiabatic indices γ approach 1, c (from γ_2) becomes very large, $4/c$ in the above expression for $f(m)$ approaches 0, as does κ_T/c, and κ_P is always positive. The contribution of low γ is called the γ-mechanism, which often acts together with the κ-mechanism. Ionizing regions do not heat up when compressed. Also in ionization zones, ionizing the gas reduces the opacity and causes a contraction of the star.

After the contraction, the ion recombines, the opacity rises, flux is absorbed, etc. Thus an ionizing zone with radiative transfer can become unstable to pulsations.

It is very complicated to evaluate the total effect of this over the entire star, as some regions drive and others damp the pulsations.

While normally the ionization zone of He II is the crucial one, in certain cases the κ-mechanism can be driven by ionization of Fe group elements. This can occur if suitable diffusion (gravitational settling) enhances the abundance of these elements by large factors (at least several powers of 10) within the star at crucial radii.

In principle, variation of nuclear energy generation rates in the core could drive a thermal cycle and produce pulsations, but as discussed above, the amplitude of waves in the core is much lower than in the higher layers, and this potential mechanism does not appear to be causing pulsation in any known category of stars.

The low amplitude non-radial oscillations seen in the Sun, and also in most similar stars that have been studied in sufficient detail, are presumably excited by stochastic variations arising within a convection zone. We expect, and observations seem to bear this out, that any star with onvection zone near its surface, will show low amplitude non-radial oscillations.

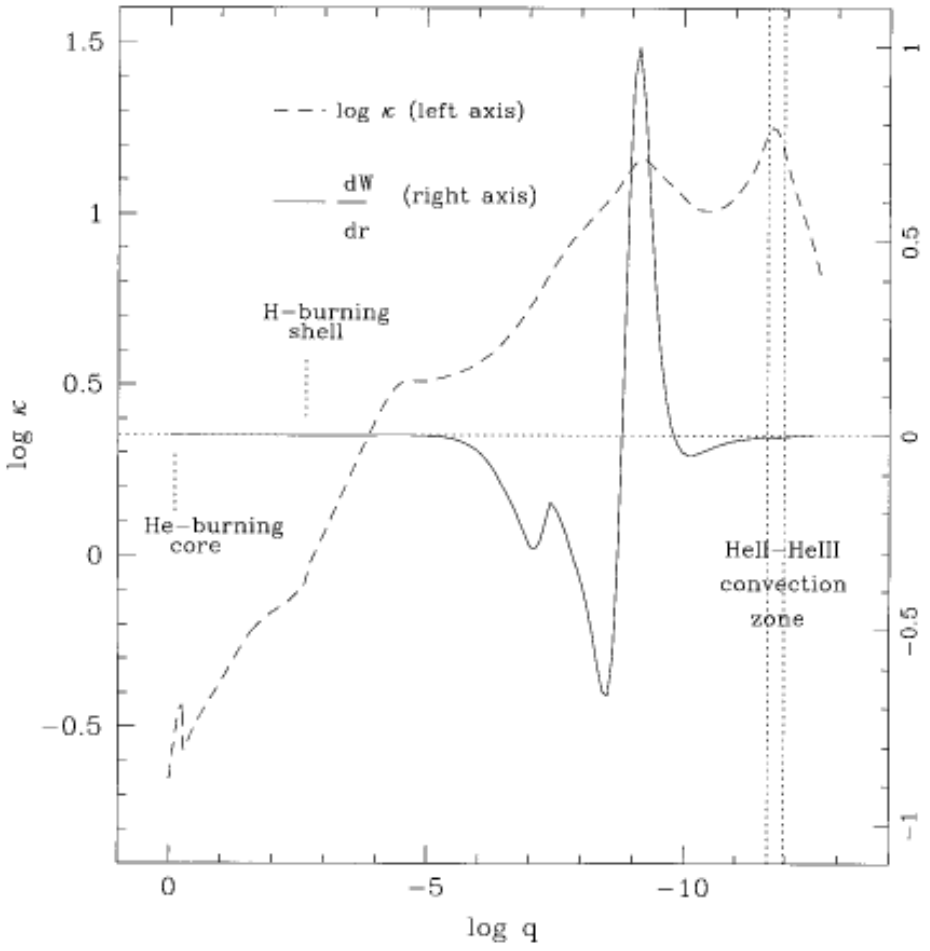

FIG. 1.—Run of the integrand of the work integral for the f-mode with $l = 2$ (*solid curve*) and of the Rosseland opacity (*dashed curve*) vs. fractional mass depth in a typical subdwarf B model. The locations of the He-burning core, the residual H-burning shell, and the He II–He III convection zone are indicated. The driving region (positive values of dW/dr) is clearly associated with an opacity bump, itself caused by heavy-element ionization.

Fig. 20.— Predicted Fe abundance and Rosseland mean opacity as a function of fractional mass depth q ($q = log[1 - M(r)/M_*]$ for a model of a subdwarf B star. Unlike the paper from which the next figure was taken, this paper was written after the predicted oscillations in this type of star had been observed. Opacity bumps are from ionization of FeII (deeper one) and from ionization of H (closer to stellar surface). (From Charpinet et al, 1997, ApJL, 483, L126)

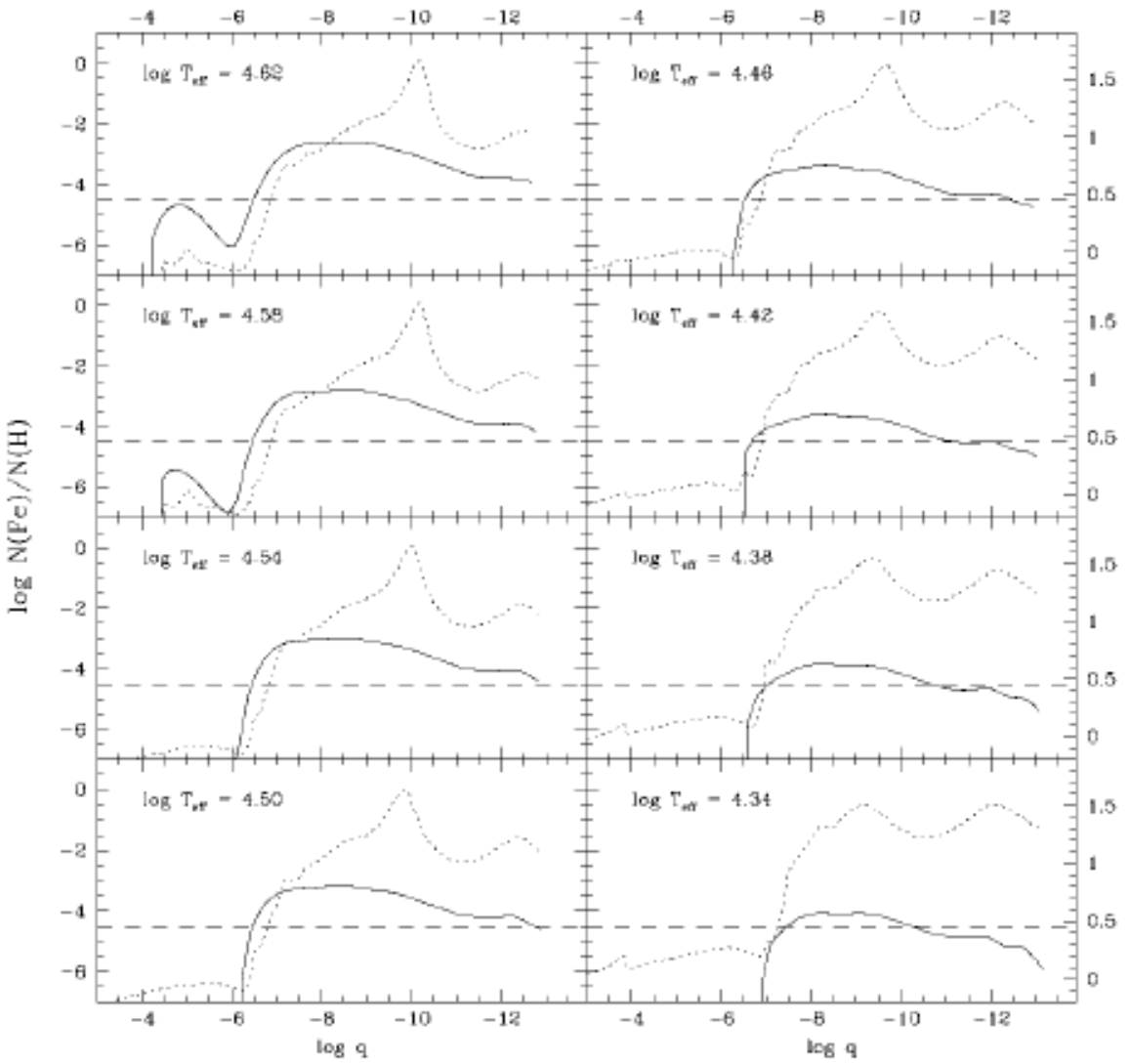

FIG. 1.—Equilibrium abundance of iron (*solid curve*) as a function of the fractional mass depth $\log q$ [$= \log (1 - M(r)/M_*)$] for a series of representative models of sdB stars with $M = 0.48\ M_\odot$, $\log g = 5.8$, and $\log T_{\rm eff}$ from 4.34 to 4.62 in steps of 0.04. In each panel the tip of the solid curve on the right hand side corresponds to the location of the Rosseland photosphere. The dashed horizontal line gives the normal value of the *Fe/H* number ratio. Also shown is the profile of the Rosseland opacity (*dotted curve*); its logarithmic value can be read on the right axis.

Fig. 21.— Predicted driving and damping regions for subdwarf B stars from Charpinet et al, (1996, ApJL, 471, L103) They predicted oscillations would be found in such stars BEFORE any asteroseismology observations of them had been made.

5. Taxonomy of Pulsating Stars

Normal radial pulsators, which have the largest amplitude of integrated light and radial velocity variations, obey $\Pi \sqrt{< \rho >} =$ constant. Since $< \rho >= (4\pi/3)M/R^3$ and $L = 4\pi R^2 \sigma T_{eff}^4$, we get

$$< \rho > \ \propto \ M \ [\frac{T_{eff}^4}{L}]^{3/2}, \qquad \frac{\Pi \sqrt{M} \ T_{eff}^3}{L^{3/4}} \ = \ \text{constant.}$$

Thus for homologous stars, where M and T_{eff} and L are all related to each other by power laws, we end up with a period – luminosity law, valid for a particular type of variable star within a small range of M and T_{eff}.

Determining the $\Pi - L$ law for Galactic Cepheids is difficult because these stars are bright, hence distant, and in the Galactic plane. In many cases they are too distant for parallaxes and their reddenings are high. A recent discussion of these issues together with the latest calibrations can be found in Fouque, Arriagada, Storm et al, 2007, A&A (in press) (see Astro-ph/0709.3255)

These period–luminosity laws have been very important in establishing distances to various types of variable stars, predominantly Cepheids and RR Lyr stars, which can be found and monitored in nearby galaxies with ground based telescopes in sites with good seeing (for the nearest galaxies) or with HST for somewhat more distant ones. This in turn is a key step in the distance ladder for more distant galaxies, determining the Hubble constant, etc. There are several factors such as metallicity which have small effects on the period – luminosity relation which must be taken into account for accurate distance determinations.

Radial pulsators include the δ Scuti stars, the Cepheids and RR Lyrae stars (both of which can be double mode pulsators in narrow ranges of ΔL and ΔT_{eff}. These stars

are crossing the instability strip (the region where radial pulsation can occur is a strip in the HR diagram slanting from high L, lower T_{eff} to lower L and higher T_{eff}, see the appended figure) for the second time. Third crossing Cepheids are called BL Her stars, higher crossings are called W Vir stars. Then there are the semi-regular and Mira variables, cool and with high luminosities.

The position of the instability strip in the H-R ($L - T_{eff}$) diagram is derived in § 8.2.3 of HKT. The arguement involves the depth within the star of He II ionization region, a location in msass ΔM below the surface of the star. The temperature at that depth is fixed by the requirements for ionization of He II to be ocurring. The pressure at that depth is fixed by having to support the overlying mass ΔM. The region must also be located where the thermal timescale becomes approximately equal to the dynamical timescale, so that in the deeper layers pulsations are adiabatic, but at the transition layer and higher, the pulsations are not adiabatic as the thermal timescale is small due to the low density. From this, the location of the instability strip as a function of stellar luminosity and T_{eff} can be derived. One gets for the predicted instability strip

$$L \propto T_{eff}^{-20},$$

close to the very steep observed instability strip of fundamental mode pulsators. Adding in an expression for the luminosity of a He-core burning star in the region of the instability strip from stellar models (HKT adopts $L \propto M^{9/2}$, one can predict (roughly) the period – radius and period – luminosity laws, $\Pi \propto R^{1.31}$ and $\Pi \propto L^{0.79}$, both of which are close to the observed properties of fundamental mode pulsators such as Cepheid variables.

The ratios of periods for stars pulsating in two modes, i.e. the fundamental and first overtone radial modes, is a key test of pulsation theory and of stellar models. Another key test is to compare evolutionary masses for stars of known distance with the pulsational

masses (usually applied to Cepheids). Until recently this gave problems at the level of a factor of $\sim 40\%$, with the pulsational masses being smaller. The pulsational models used generally ignore convective overshoot. Recently Keller & Wood (2006, ApJ, 642, 834) suggest that enhanced internal mixing near the boundaries of the convective zones may resolve this problem.

Mira variables (luminous AGB stars) as they evolve up the AGB become pulsationally unstable. They begin pulsating in the first overtone, but as they evolve up the AGB to still higher L, they switch to the fundamental mode. At that time the pulsation amplitude becomes very large, substantial mass loss then follows, and the stars become obscured by the ejected material at optical wavelengths, but very bright in the infrared. (see papers on OH/IR stars by Wood and others)

Observations of light curves for many bright high amplitude variable stars have been obtained for many years; the best cases are photometrically monitored by the AAVSO (American Association of Variable Star Observers, a group of amateur astronomers), which can supply light curves for some variable stars extending over 25 years or more. Cepheids, for example, may vary in light at V by about 1 mag, and have radial velocity variations across the cycle of ~ 50 km/sec. Period changes can be measured for many Cepheids (see, e.g. Turner et al, Astro-ph/0709.3085, where the period of the Cepheid studied, RT Aur, of 3.728 days, is increasing by 0.082 ± 0.012 sec/yr) and used to test the theory of stellar evolution and pulsational theory.

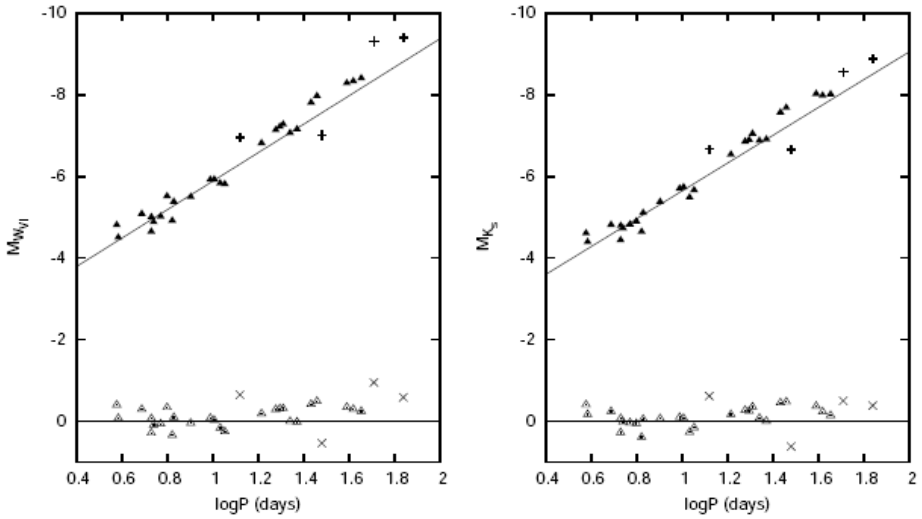

Fig. 1. Comparison of absolute magnitudes derived from ZAMS parallaxes (triangles) for 30 stars with the *PL* relations based on 54 IRSB parallaxes in W_{VI} and K_s bands (solid lines). The bottom panel shows residuals with respect to the IRSB *PL* relations. Long-period Cepheids appear to be progressively shifted. Rejected stars (see text) are marked with pluses and crosses.

Fig. 22.— Period luminosity law for Galactic Cepheids with the most accurate distances for the V and the K bandpass. The plot i log(period) vs. log(1/Luminosity) because the magnitude scale is logarithmic and inverted (smaller mag $\equiv$ fainter L). Fig. 1 of Fouque, Arriagada, Storm et al, 2007, A&A (in press) (see Astro-ph/0709.3255)

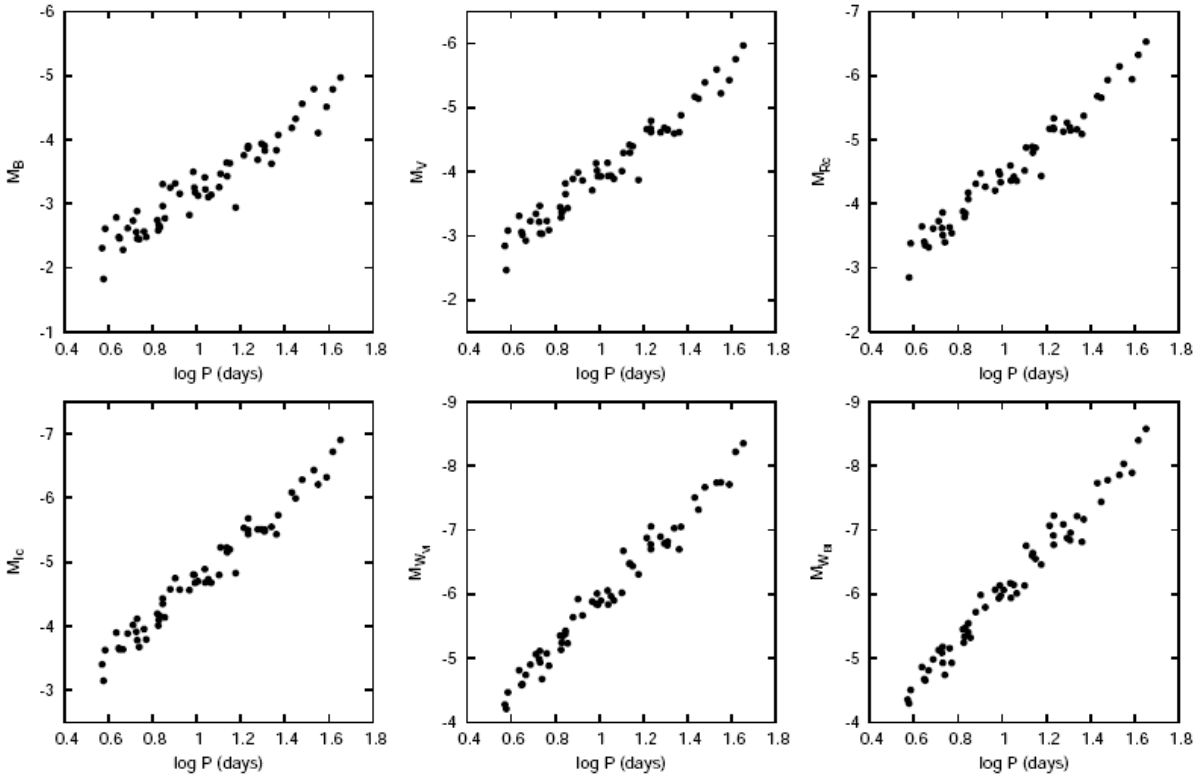

Fig. 2. Adopted Galactic *PL* relations in optical bands.

Fig. 23.— Period – luminosity relations for Galactic Cepheids using various optical bandpasses. Fig. 2 of Fouque, Arriagada, Storm et al, 2007, A&A (in press) (see Astro-ph/0709.3255)

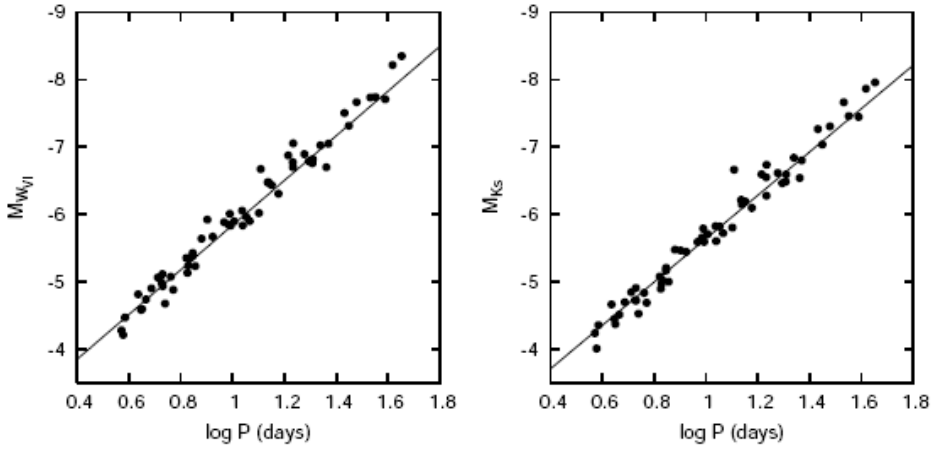

Fig. 4. Galactic *PL* relations in W_{VI} and K_s bands, superimposed with LMC Ogle relations shifted by a magnitude offset of 18.40.

Fig. 24.— Period – luminosity relations for Galactic Cepheids in V and in K bandpasses compared to that defined for Cepheids in the LMC using a mag. offset of 18.40. (Knowing the mean reddening of the LMC Cepheids, a distance to the LMC can thus be determined.) Fig. 4 of Fouque, Arriagada, Storm et al, 2007, A&A (in press) (see Astro-ph/0709.3255)

6. References and Suggested Reading

Selected recent conferences:

Astrophysics of Variable Stars, 2005, ASP Conference Series Vol. 349

International Workshop on Asteroseismology, held in Dec 2004, Journal of Astrophysics and Astronomy (India), 26, 115

Key references for early discoveries include:

Leighton, Noyes & Simon, 1962, ApJ, 135, 474

Libbrecht, Woodard & Kaufman, 1990, ApJS, 74, 1134 (first detailed mode study)

Libbrecht & Woodard, 1991, Science, 253, 152 (overview as of 1991)

More recent references:

Antia & Basu, 1996, ApJ, 426, 801 (on the Solar He content)

Lazrek, Baudin, Bertello et al, 1997, Solar Physics, 175, 227 (First results on p-modes from GOLF Experiment on SOHO)

Basu, Antia & Bogart, 2007, ApJ (in press) (see Astro-ph/0705.3154) (on the metallicity in the Solar interior as inferred using p-mode frequencies)

Tripathy, Hill, Jain & Leibacher, 2007, Solar Physics (in press) Solar Oscillation Frequency Changes...correlation with solar activity

Reviews on helioseismology:

Christensen-Dalsgaard, 2002, Reviews of Modern Physics (on helioseismology)

Cunha, Aerts, Christensen-Dalsgaard, et al, Asteroseismology and Interferometry, 2007, to be published in Astronomy & Astrophysics Review, see Astro-ph/0709.4613 (155 pages long)

Demarque & Guenther, 1999, Proc.Natl.Acad.Sciences, USA, Helioseismology: Probing the Interior of a Star

Gough & Toomre, 1991, Ann. Revs.of Astronomy and Astrophysics, 26, 627 (Seismic Observations of the Solar Interior)

Thompson et al, 2003, Annual Reviews of Astronomy and Astrophysics, 41, 299 (The internal rotation of the Sun)

Gough, 2003, Astrophysics and Space Science, 284, 165 (on the principal asteroseismic signatures)

Selected asteroseismology papers:

Kepler, Nather, Winget et al, 2003, A&A, 401, 639 (pulsating white dwarf GD 358)

Vauclair, Moskalik, Pfeiffer et al, 2002, A&A, 381, 122 (PG 1159 star)